

Frontiers in Flow Cytometry™

Annual event by Thermo Fisher Scientific

A 24 hour Virtual Event

Tuesday May 17, 2022

#FrontiersInFlow

ThermoFisher
SCIENTIFIC

WILEY



Frontiers in Flow Cytometry™

A 24 hour Virtual Event by Thermo Fisher Scientific

Want to discover the latest advances in strategies & applications in flow cytometry?

Frontiers in Flow Cytometry is aimed at researchers across the globe looking for an opportunity to share current developments in flow cytometry.

Key topics include:

- Spectral and conventional flow cytometry
- Immunophenotyping
- Panel design and optimization
- Infectious diseases
- Advances in flow cytometry technology

This 24 hour virtual event will feature keynote presentations and industry colleagues, webinars, demos, live networking opportunities and more.

Join the conversation with your colleagues around the world. We are kicking off the event on May 17 at 8am SGT; 2am CEST; and 5pm PDT (May 16th).

#FrontiersInFlow

REGISTER NOW

Transcriptome-based screening of ion channels and transporters in a migratory chondroprogenitor cell line isolated from late-stage osteoarthritic cartilage

Csaba Matta^{1,2}  | Rebecca Lewis²  | Christopher Fellows² | Gyula Diszhazi³ | Janos Almassy³ | Nicolai Miosge⁴ | James Dixon⁵  | Marcos C. Uribe⁶  | Sean May⁶  | Szilard Poliska⁷  | Richard Barrett-Jolley⁸  | Janos Fodor³ | Peter Szentesi³  | Tibor Hajdú¹ | Aniko Keller-Pinter⁹  | Erin Henslee¹⁰ | Fatima H. Labeed¹⁰  | Michael P. Hughes¹⁰  | Ali Mobasher^{11,12,13,14} 

¹Department of Anatomy, Histology and Embryology, Faculty of Medicine, University of Debrecen, Debrecen, Hungary

²Department of Veterinary Preclinical Sciences, School of Veterinary Medicine, Faculty of Health and Medical Sciences, University of Surrey, Guildford, UK

³Department of Physiology, Faculty of Medicine, University of Debrecen, Debrecen, Hungary

⁴Department of Prosthodontics, Tissue Regeneration Work Group, Georg August University, Göttingen, Germany

⁵Wolfson Centre for Stem Cells, Tissue Engineering and Modelling, Centre of Biomolecular Sciences, School of Pharmacy, University of Nottingham, Nottingham, UK

⁶The Nottingham Arabidopsis Stock Centre (NASC), School of Biosciences, University of Nottingham, Sutton Bonington Campus, Loughborough, UK

⁷Genomic Medicine and Bioinformatic Core Facility, Department of Biochemistry and Molecular Biology, Faculty of Medicine, University of Debrecen, Debrecen, Hungary

⁸Department of Musculoskeletal Biology, Faculty of Health and Life Sciences, Institute of Ageing and Chronic Disease, University of Liverpool, Liverpool, UK

⁹Department of Biochemistry, Faculty of Medicine, University of Szeged, Szeged, Hungary

¹⁰Department of Mechanical Engineering Sciences, Centre for Biomedical Engineering, University of Surrey, Guildford, UK

¹¹Department of Regenerative Medicine, State Research Institute Centre for Innovative Medicine, Vilnius, Lithuania

¹²Research Unit of Medical Imaging, Physics and Technology, Faculty of Medicine, University of Oulu, Oulu, Finland

¹³Departments of Orthopedics, Rheumatology and Clinical Immunology, University Medical Center Utrecht, Utrecht, The Netherlands

¹⁴Department of Joint Surgery, The First Affiliated Hospital, Sun Yat-sen University, Guangzhou, China

Correspondence

Csaba Matta, Department of Anatomy, Histology and Embryology, Faculty of Medicine, University of Debrecen, Debrecen H-4032, Hungary.
Email: matta.csaba@med.unideb.hu

Abstract

Chondrogenic progenitor cells (CPCs) may be used as an alternative source of cells with potentially superior chondrogenic potential compared to mesenchymal stem cells (MSCs), and could be exploited for future regenerative therapies targeting articular cartilage in degenerative diseases such as osteoarthritis (OA). In this study,

Abbreviations: AD-MSC, adipose tissue-derived mesenchymal stem cell; BK, large conductance calcium-activated potassium channel; BM-MSC, bone marrow-derived mesenchymal stem cell; CPC, chondrogenic progenitor cell; DEP, dielectrophoresis; ECM, extracellular matrix; GAG, glycosaminoglycan; IBTX, iberiotoxin; MSC, mesenchymal stem cell; OA, osteoarthritis; PCA, principal component analysis; PG, proteoglycan; RMP, resting membrane potential; SOCE, store-operated Ca²⁺ entry; TRP, transient receptor potential.

Csaba Matta and Rebecca Lewis should be considered as joint first author.

This is an open access article under the terms of the Creative Commons Attribution License, which permits use, distribution and reproduction in any medium, provided the original work is properly cited.

© 2021 The Authors. *Journal of Cellular Physiology* published by Wiley Periodicals LLC

Ali Mobasher, Department of Regenerative Medicine, State Research Institute Centre for Innovative Medicine, Vilnius, Lithuania.
Email: ali.mobasher@oulu.fi

Funding information

FP7 People: Marie-Curie Actions, Grant/Award Number: 625746; National Research, Development and Innovation Fund, Hungary, Grant/Award Number: TKP2020-NKA-04; FP7 Health, Grant/Award Number: 305815; Eötvös Loránd Research Network (ELKH), Grant/Award Number: 460043; European Structural and Social Funds, Research Council of Lithuania, Grant/Award Number: DOTSUT-215; Deanship of Scientific Research, King AbdulAziz University, Grant/Award Number: 1-141/1434 HiCi; Premium Postdoctoral Research Fellowship, Hungarian Academy of Sciences; National Research, Development and Innovation Office, Hungary, Grant/Award Number: FK 134304, FK 134684; Arthritis Research UK, Grant/Award Number: 20194; Attracting Foreign Researchers for Research Implementation, Grant/Award Number: 01.2.2-LMT-K-718-02-0022

we hypothesised that CPCs derived from OA cartilage may be characterised by a distinct channelome. First, a global transcriptomic analysis using Affymetrix microarrays was performed. We studied the profiles of those ion channels and transporter families that may be relevant to chondroprogenitor cell physiology. Following validation of the microarray data with quantitative reverse transcription-polymerase chain reaction, we examined the role of calcium-dependent potassium channels in CPCs and observed functional large-conductance calcium-activated potassium (BK) channels involved in the maintenance of the chondroprogenitor phenotype. In line with our very recent results, we found that the *KCNMA1* gene was upregulated in CPCs and observed currents that could be attributed to the BK channel. The BK channel inhibitor paxilline significantly inhibited proliferation, increased the expression of the osteogenic transcription factor *RUNX2*, enhanced the migration parameters, and completely abolished spontaneous Ca^{2+} events in CPCs. Through characterisation of their channelome we demonstrate that CPCs are a distinct cell population but are highly similar to MSCs in many respects. This study adds key mechanistic data to the in-depth characterisation of CPCs and their phenotype in the context of cartilage regeneration.

KEYWORDS

cartilage, channelome, chondrocyte, chondroprogenitor, mesenchymal stem cell, osteoarthritis, transcriptomics

1 | INTRODUCTION

The prevalence of musculoskeletal conditions is constantly increasing, making age-related and chronic inflammatory joint diseases the major causes of disability in the elderly population (Al Maini et al., 2020). Osteoarthritis (OA) is the most common form of chronic musculoskeletal disorders (Hunter & Bierma-Zeinstra, 2019). Although the primary target of OA is articular cartilage, it also affects other tissues within and around the joint (Loeser et al., 2012). The affected tissues undergo metabolic, structural and functional alterations that contribute to joint pain, disease progression and patient disability (Henrotin et al., 2016).

Chondrocytes are the main cell type in articular cartilage (Archer & Francis-West, 2003), along with a scarce population of cartilage progenitor cells (CPCs) (Nakayama et al., 2020). The resident cells are embedded in a cartilage-specific extracellular matrix (ECM) that consists of collagen type II, large aggregating proteoglycans (PG; e.g., aggrecan), constituent glycosaminoglycans (GAG), hyaluronan, small PGs and other collagenous and noncollagenous proteins (Buckwalter et al., 2005). A high amount of interstitial water (~80% of the total weight of cartilage) is osmotically drawn to the freely mobile cations (i.e., Na^+ , K^+ , Ca^{2+}) balancing the negatively charged GAG side chains of PGs and are therefore present at high local concentrations. Cells in cartilage ECM are thus exposed to a unique ionic microenvironment (Mobasher et al., 1998; Urban et al., 1993). Cartilage is avascular, and as a consequence of the scarcity of available nutrients and

oxygen, it is unique, relatively hypoxic and acidic milieu, as well as low cellularity, it is incapable of mounting a sufficient healing and repair response following injury (Gomoll & Minas, 2014).

The presence of a cartilage-specific CPC population with stem cell properties in the superficial zone of articular normal cartilage is now widely accepted (Dowthwaite et al., 2004). More recently, cells in OA articular cartilage with mesenchymal progenitor cell characteristics have also been observed and characterised (Fellows et al., 2017). These cartilage progenitor/stem cell populations have the potential for chondrogenic induction and trilineage plasticity. CPCs have also been described in late-stage OA cartilage, which is believed to be migrating in response to chemotactic signals from the bone marrow through breaks in the tide mark, as an attempt to regenerate damaged cartilage ECM (Koelling et al., 2009). However, knowledge concerning the specific phenotypic features and regenerative potentials of chondroprogenitor cells is still incomplete. CPCs are considered an ideal source for cell-based cartilage repair, and therefore progress has been made in identifying, understanding and characterising these cells.

In OA, chondrocytes and CPCs exist in a microenvironment dominated by mediators that promote matrix degradation and low-grade inflammation. There is evidence that cartilage ECM undergoes profound alterations during OA in terms of GAG and water content (Mankin & Lippiello, 1970). That in turn alters the osmolality of the matrix and the composition of the unique ionic milieu (Mow et al., 1999). Chondrocytes and other cells in cartilage respond

to these changes and maintain their homeostasis by altering the transport of ions across the cell membrane (Hdud et al., 2014) via transporters and ion channels, collectively referred to as the 'channelome' (Asmar et al., 2016; Barrett-Jolley et al., 2010; Mobasher et al., 2019).

Plasma membrane transporters including voltage-gated sodium, potassium and calcium channels, chloride channels, calcium-activated potassium channels, transient receptor potential (TRP) channels, N-methyl-D-aspartate receptors and purinergic receptors have been described in chondrocytes, which allow them to respond to the local ionic composition of the pericellular matrix by adjusting the resting membrane potential (RMP) (Maleckar et al., 2020), which has been shown to play a crucial role in regulating metabolic activity and synthetic rate of cartilage ECM, as well as proliferation, differentiation or volume regulation (Asmar et al., 2016; Matta & Zakany, 2013; Mobasher et al., 2019). Although much progress has been made towards characterising the chondrocyte channelome, many open questions remain concerning the composition of the ion channel complement and their function in chondroprogenitor cells. Whilst there is accumulating data suggesting that several genes encoding ion channels which are involved in the regulation of mechanotransduction, cell volume, RMP and apoptosis are differentially expressed in OA chondrocytes (Lewis & Barrett-Jolley, 2015), current understanding concerning the channelome of CPCs, especially with regard to differentially regulated ion channel genes, is incomplete. Addressing this gap in knowledge is a high priority for the identification and targeting of new therapeutic targets for the treatment of OA.

In this study, we hypothesised that CPCs derived from OA cartilage may be characterised by a different assembly of ion channels and transporters that regulate their function and phenotype and maintain communication with the altered ECM. Given that there is some evidence that migratory CPCs are related to mesenchymal stem cells (MSCs) residing in the bone marrow close to the subchondral bone which has migrated to lesioned cartilage through breaks in the tide mark, we used bone marrow-derived MSCs (BM-MSCs) as a reference cell population. We have recently analysed the surfaceome of CPCs using selective cell surface protein labelling followed by quantitative high-throughput mass spectrometry and identified alterations in the composition of the surfaceome compared to MSCs (Matta et al., 2019). However, even that approach was not sensitive enough to detect alterations in very low-abundance ion channels or other transporters. In this study, we attempted to differentiate CPCs from BM-MSCs based on their transcriptome and electrophysiological properties. We first performed a global transcriptomic analysis using Affymetrix microarrays. We studied the profiles of those ion channels and transporter families that are known to be involved in regulating chondrocyte physiology, RMP, volume regulation, calcium signalling, matrix secretion or chondrogenesis, which may have relevance in chondroprogenitor cell physiology (Barrett-Jolley et al., 2010; Matta & Zakany, 2013; Mobasher et al., 2019; Suzuki et al., 2020). We then employed patch clamping and dielectrophoresis (DEP) to characterise the basic

electrophysiological profile (the 'electrome'; De Loof, 2016) of the two cell types. Following validation of the microarray data using quantitative real-time polymerase chain reaction (RT-qPCR), we examined the role of calcium-dependent potassium channels in the cellular physiology and homeostasis of migratory CPCs and found that the large-conductance calcium-activated potassium channels (BK) are functionally expressed and are involved in the maintenance of the chondroprogenitor phenotype.

2 | MATERIALS AND METHODS

2.1 | Cell culture

Experiments were carried out on a human migratory CPC cell line derived from late-stage OA knee articular cartilage, which has been immortalised by viral transfection of the human telomerase reverse transcriptase (hTERT) as previously described (Koelling et al., 2009). CPCs were cultured in monolayers in 75 cm² cell culture flasks (Nunc; Thermo Fisher Scientific) until approximately 80% confluence in GlutaMax DMEM (1.0 g/L glucose; Gibco; Thermo Fisher Scientific) containing 10% foetal calf serum (FCS; Gibco) and 50 µg/ml gentamycin (Sigma-Aldrich). As a reference cell population, human BM-MSCs (Lonza) were used. The cells were received at passage 2 and were expanded until passage 4 in Lonza hMSC medium at 37°C in a humidified atmosphere of 5% CO₂. MSCs were hTERT-immortalised as previously described (Okamoto et al., 2002) with the modifications detailed in (Saeed et al., 2015). Immortalised MSCs were expanded in monolayers in 75 cm² cell culture flasks (Nunc) until approximately 80% confluence in GlutaMax DMEM (4.5 g/L glucose; Gibco) containing 10% FCS (Gibco) and 1% P/S (Sigma-Aldrich).

2.2 | RNA isolation and reverse transcription

Total RNA was isolated from cells grown in monolayers in 75 cm² cell culture flasks using the RNeasy kit (Qiagen) as per the instructions of the manufacturer and stored at -80°C. RNA concentration and purity were determined by a NanoDrop 2000 UV-Vis spectrophotometer (Thermo Fisher Scientific). For gene expression analyses, 2 µg of RNA was reverse-transcribed into complementary DNA (cDNA) using the High-Capacity cDNA Reverse Transcription Kit (Thermo Fisher Scientific), following the protocol supplied by the manufacturer. cDNA was stored at -20°C.

2.3 | Affymetrix microarray analysis

RNA integrity was confirmed using an Agilent 2100 Bioanalyzer with the RNA 6000 Nano Kit (Agilent Technologies). The RNA integrity numbers were ≥9.6 for all samples. Whole-genome transcriptome analysis was conducted by hybridising three biological samples of total RNA per cell type to Affymetrix Human Gene 2.1 ST Arrays Strips (Affymetrix).

All steps were conducted at the Nottingham Arabidopsis Stock Centre. Gene expression data were analysed using Partek Genomics Suite 6.6 software (Partek Incorporated). The raw CEL files were normalised using the RMA background correction with quantile normalisation, log base 2 transformation and mean probe-set summarisation with adjustment for GC content. Differentially expressed genes (DEG) were identified by a two-way analysis of variance, and *p* values were adjusted using the false discovery rate (FDR) method to correct for multiple comparisons. DEG was considered significant if *p* value with FDR was ≤ 0.05 . The expression data of genes coding for selected transporter and ion channel subunits are summarised in Tables S1–S4. The data set is published in a MIAME compliant format in the GEO database (<http://www.ncbi.nlm.nih.gov/geo/>); accession numbers: GSM4885525–GSM4485530 (GSE160886).

2.4 | Pathway analysis

CytoScape v3.4 software with ClueGo v2.3.5 application was used for identifying overrepresented gene ontology (GO) terms. A two-sided hypergeometric test with Bonferroni step-down correction was performed using the list of DEG and the GO Biological process database.

2.5 | RT-qPCR analyses

Selected ion channel subunit genes were analysed by RT-qPCR using a custom configured TaqMan 96-Well Fast Gene Expression Array plate (see Tables S5 and S6) and then by absolute quantification using the standard curve method. Primer pairs were ordered from Eurogentec. For sequences of primer pairs please see Table S7. First, standard curves had been generated by conventional PCR using the Promega GoTaq Flexi DNA Polymerase kit (Promega) by adding the following components (per 50 μ l reaction): 1.25 U GoTaq polymerase, 3 mM MgCl₂, 0.2 mM dNTP, 200 nM primers and 10 ng cDNA. Amplification was performed in a Techne Prime Thermal Cycler (Techne; Bibby Scientific Ltd) using the following thermal profile: initial denaturation at 95°C for 5 min, followed by 40 cycles of denaturation at 95°C for 15 s, annealing at 58°C for 20 s, extension at 74°C for 20 s, and then final extension at 74°C for 5 min. PCR products were isolated using a Roche High Pure PCR Product Purification Kit (Roche) according to the instructions of the manufacturer. DNA concentration of purified PCR products was determined using a NanoDrop 2000 UV-Vis spectrophotometer (Thermo Fisher Scientific). Standard curves were prepared by a serial (10-fold) dilution starting from 1 ng/ μ l.

RT-qPCR reactions were set up using the Promega GoTaq qPCR Master Mix and 20 ng input cDNA per each 10- μ l reaction. Reactions were run in a Techne Prime Pro 48 Real-time qPCR machine using the following thermal profile: activation and initial denaturation at 95°C for 10 min, followed by 40 cycles of denaturation at 95°C for 10 s, annealing at 58°C for 30 s, extension at 72°C for 20 s, and then final extension at 72°C for 20 s. Due to spatial limitations in the 48-well

qPCR plates, quantification of qPCR products was performed by absolute quantification using the standards prepared in the previous step, followed by normalising the expressional data of genes of interest to those of the most stably expressed reference gene (*PPIA*), and then the expression levels for the genes were normalised to those in MSCs (set at 1.0). The optimal normalisation gene was selected using the NormFinder algorithm (Andersen et al., 2004). RT-qPCR reactions were performed on three biological replicates (*N* = 3).

2.6 | Cell proliferation and mitochondrial activity assays

To assess the effect of BK channel modulators, cells were plated into 96-well plates at a density of 5000 cells/well. Before the assays, cells were incubated for 48 h in the presence of the selective BK channel blocker iberiotoxin (IBTX) (100 nM; Tocris; Bio-Techne); the potent BK channel inhibitor paxilline (1 μ M); the BK channel activator NS1619 (10 μ M; Sigma-Andrich); or vehicles at equal volumes (water, dimethyl sulfoxide and ethanol, respectively). The rate of cell proliferation was determined by detecting the amount of incorporated radioactivity from ³H-thymidine. One microcurie per millilitre ³H-thymidine (diluted from methyl-³H-thymidine; 185 GBq/mM; Amersham Biosciences) was added to each well (Wallac, PerkinElmer Life and Analytical Sciences) for 24 h. After washing with phosphate-buffered saline (PBS), proteins were precipitated with ice-cold 5% trichloroacetic acid and rinsed with PBS again. Cells were then air-dried and radioactivity was counted by a liquid scintillation counter (Chameleon; Hidex). Measurements were carried out in seven samples of each experimental group (*n* = 7) in three independent experiments (*N* = 3). For mitochondrial activity assays, 10 μ l 3-(4,5-dimethylthiazol-2-yl)-2,5-diphenyltetrazolium bromide (MTT) reagent (thiazolyl blue tetrazolium bromide; 5 mg MTT/ml PBS; Sigma-Aldrich) was pipetted into each well. Cells were incubated for 2 h at 37°C, and following the addition of 500 μ l MTT solubilizing solution, optical density was measured at 570 nm (Chameleon; Hidex).

2.7 | Migration assays

2.7.1 | Boyden chemotaxis chamber

CPCs were washed twice in PBS, harvested with 0.25% trypsin (Sigma-Aldrich) and resuspended in a culture medium. The lower wells of a 48-well Boyden chemotaxis chamber (Neuro Probe Inc.) were filled with 1 μ l/ml human fibronectin (Sigma-Aldrich) dissolved in PBS and covered with a polycarbonate filter (Neuro Probe Inc.) containing pores with a diameter of 3 μ m. Cell suspension (50 μ l) at a density of 2×10^5 cells/ml was inoculated into the wells on the top of the membrane and the chamber was incubated for 5 h at 37°C in a humidified atmosphere with or without 1 μ M paxilline. Nonmigrated cells were removed from the *cis*-surface of the membrane and after fixation in methanol, migrated cells were stained with 1% toluidine

blue (Sigma-Aldrich) dissolved in water. Membranes were air-dried and mounted with Pertex medium (Sigma-Aldrich). Toluidine blue-stained migratory cells were counted on the trans surface of the membrane by an internally developed MATLAB (Mathworks Inc.) application. Cells were defined by an approximate range of values in the RGB colour space with a particle size of at least 30 pixels. Other structures, primarily membrane pores, cell debris and staining artefacts, were omitted based on their different overall size and their distinct position in the RGB colour space. Cells in six wells were counted in each experimental group and three independent assays ($N = 3$) were performed.

2.7.2 | Time-lapse imaging of live cells

Live-cell imaging was carried out using the CytoSMART 2 imaging system (CytoSMART Technologies). For imaging, cells were seeded in 35-mm Petri dishes at a density of 1×10^4 cells. After allowing the cells to adhere for 120 min, the Petri dishes were transferred onto the device and imaging has started, either with or without $1 \mu\text{M}$ paxilline. Phase-contrast time-lapse images were obtained automatically at 30-min intervals for 18 h at 37°C and 5% CO_2 . Time-lapse images were analysed using ImageJ (National Institutes of Health; <https://imagej.nih.gov/ij/>) and CellTracker (<http://celltracker.website/>) software programmes. The cells were tracked manually through every frame, and the x and y coordinates of the movements were recorded. We excluded dying, dividing or damaged cells from the analysis. The length of the total path, maximal distance from the origin, as well as average and maximum cell speeds were calculated. To create wind rose plots illustrating the trajectories, the migratory tracks of the individual cells were shifted to a common origin. Three independent experiments ($N = 3$) were performed.

2.8 | Electrophysiology

2.8.1 | DEP

Cells were grown to approximately 80% confluence before analysis. Cells were dissociated from the culture plates by trypsinisation. Afterwards, cells were washed twice and resuspended in an isotonic DEP medium with low ionic strength containing 8.5% (wt/vol) sucrose (Sigma-Aldrich), 0.3% (wt/vol) glucose (Sigma-Aldrich), and adjusted to a final conductivity of 10 mS/m using PBS (Sigma-Aldrich). Buffer conductivity was measured with a conductivity metre (RS Components Ltd). Cell counts and viability for each experiment were determined using a haemocytometer and trypan blue, which indicated a $96 \pm 2\%$ viability. To reduce the effect of variation in cell numbers in each sample, the final cell concentration was adjusted to 5×10^5 cells/ml.

DEP spectra were obtained using the 3DEP DEP-Well system (DEPtech), as described in more detail earlier (Labeed et al., 2011). Briefly, cells resuspended in DEP media were administered into the

wells of DEP-Well chips containing 12 ring-shaped, $17\text{-}\mu\text{m}$ wide, gold-plated copper electrodes around the good circumference with gaps of $75 \mu\text{m}$ between electrodes, and energised with currents at specific frequencies. The DEP method is based on the principle that the cells are either attracted or repelled from the side of the well by an amount proportional to their polarizability, as described previously (Hoettges et al., 2019).

Changes in light intensity across the wells over time were determined using a 1.3 MegaPixel video camera installed on the microscope and a MATLAB (Mathworks Inc.) script. The change in cell distribution was monitored by recording an image every 3 s for a total of 30 s. The entire well was divided into 10 segments that were monitored separately; however, only segments 7–9 were analysed as previously described (Hoettges et al., 2008). The wells were energised with frequencies ranging from 1 kHz–20 MHz at five points per decade. Spectra were generated using MATLAB (Mathworks Inc.) and presented in values of light intensity versus frequency. Light intensity data were fit to the single-shell model (Broche et al., 2005) and the best-fit model was used to determine the following features: specific membrane capacitance (C_{Spec}), specific membrane conductance (G_{Spec}) and crossover frequency (i.e., the frequency where the DEP force is zero). The best-fit model (highest Pearson correlation coefficient) was established by matching the curve to the measured data and adjusting the dielectric cytoplasmic and membrane parameters until the best match was found. MATLAB scripts were used for all images as well as for signal processing and data analysis as previously described (Hoettges et al., 2008). Given that the key parts of the DEP curve (starting and end values and transition frequencies) can be associated with the membrane capacitance and conductance and cytoplasm conductivity and permittivity, these parameters were determined uniquely by fitting the curve to the data points. Cell diameters were measured in a haemocytometer and the average radius was calculated using ImageJ software version 1.51 (<http://imagej.nih.gov/ij/>); the mean radii were used for the DEP model. All experiments were repeated three times ($N = 3$ independent experiments); data are expressed as mean \pm SD.

2.8.2 | Patch clamp

Whole-cell currents were measured under voltage-clamp conditions as described earlier (Almassy & Begenisich, 2012). Extracellular solution contained (in mM): NaCl, 140; KCl, 5; CaCl_2 , 2; MgCl_2 , 1; HEPES, 10; glucose, 5; pH 7.4 with NaOH. Patch pipettes were fabricated from thick-walled borosilicate glass (o.d. 1.5 mm, i.d. 0.85 mm) with the resistance of approximately $5 \text{ M}\Omega$ when filled with intracellular solution. The pipette solution contained (in mM): D-gluconic acid potassium salt, 115; KCl, 26; MgCl_2 , 1; EGTA, 5; HEPES, 10; pH 7.2 with KOH. The specific BK channel inhibitor paxilline (Alomone Labs) was used in $5 \mu\text{M}$ to verify the functional expression of the channels. V_m values were determined following 2 min of stable membrane potential recording with $I = 0$ on Axon 200 A/B amplifiers (Lewis et al., 2011). Only cells with seal resistance

above 10 G Ω and good access ($R_s < 20$) were used. Whole-cell currents were recorded in $n = 27$ CPC and 7 MSC cells. For RMP measurements, all values are quoted as mean \pm SEM, with sample size (n) = 22 (CPC) and 8 (MSC). All membrane potentials are corrected for liquid junction potentials estimated using JPCalc (Barry & Lynch, 1991).

2.9 | Measurement of intracellular Ca²⁺ oscillations in CPCs

Cells were loaded with 10 μ M Fura-2-AM for 50 min at 37°C in a CO₂ incubator. After loading, cells were kept in Tyrode's solution and placed on the stage of a ZEISS Axiovert 200M inverted microscope (Zeiss) equipped with a Plan-Neofluar $\times 20$ objective (NA = 0.5). Fura-2 was excited with a CoolLED pE-340fura light source (CoolLED Ltd.). Illumination was alternating between 340 and 380 nm wavelength and the emitted fluorescent light was measured through a band-pass filter (505–570 nm) and digitised at 16 bit with an AXIOCam MR3 monochrome camera (Zeiss) at a frequency of 12 frames/min. Image acquisition and postprocessing were carried out with the AxioVision (rel. 4.8) software (Zeiss). The cells were examined in resting conditions for 15 min at room temperature. At the end of the experiments, 180 μ M ATP was added to the bath to check the viability of the cells. Cells not responding to the ATP challenge were excluded from the analysis. Intracellular Ca²⁺ concentration ([Ca²⁺]_i) was calculated from the ratio of the images taken at 340 and 380 nm after background correction with constants determined during in vitro calibration of the setup. The cells were classified as active if the increase of [Ca²⁺]_i was more than 10% of the resting level. $n = 332$ cells were analysed.

2.10 | Statistical analysis

All data are representative of at least three independent experiments (biological replicates). RT-qPCR, cell proliferation and mitochondrial activity, as well as cell migration data, are expressed as mean \pm SEM, DEP data are expressed as mean \pm SD. Statistical analysis was performed using Student's unpaired two-tailed t -test (* $p < .05$; ** $p < .01$; *** $p < .001$).

3 | RESULTS

3.1 | Affymetrix analysis reveals differentially expressed ion channel genes in migratory CPCs

We performed a principal component analysis of the Affymetrix data on normalised samples to explore their interrelationships (Figure 1). Biological replicates within the CPC/MSc groups were separated into two distinct clusters, showing that the pattern of gene expression was different in CPCs and MSCs. In total, 3214 genes showed significantly different expression levels between CPC and MSC cells,

with 2379 genes being downregulated and 835 genes upregulated. Using CytoScape software with the ClueGo application we identified those GO Biological process terms which were overrepresented in our gene list. When we analysed the full gene list (up- and down-regulated genes together), and the list of downregulated genes, we found that mainly cell cycle-related categories such as cell cycle, regulation of cell cycle, cell cycle checkpoint and mitotic/meiotic cell cycle processes were enriched. Furthermore, DNA/nucleic acid metabolism-related pathways were also overrepresented. Separate analyses of upregulated genes indicated the enrichment of different types of tissue development and cell proliferation processes, such as skin development and mesenchymal cell proliferation (Figure S1 in the File S1; see also File S2).

To characterise the expression profiles of genes encoding ion channel subunits in CPCs and to identify differences in expression levels compared to MSCs, we further explored the microarray analysis data. We assessed genes encoding ion channels and transporters commonly involved in regulating potassium, sodium and chloride transport and calcium homeostasis in chondrocytes (Figure 2; see also Tables S1–S4). The expression levels for some of the genes studied were different in migratory CPCs versus MSCs. Genes encoding members of the calcium-activated potassium channels (K_{Ca}) showed the most prominent expression changes; *KCNMA1* and *KCNN4*, the genes coding for the pore-forming alpha subunit of the large-conductance calcium-activated potassium channel (K_{Ca}1.1), and the intermediate/small conductance calcium-activated potassium channel (K_{Ca}3.1), respectively. In both cases, there was a more than 1.5-fold upregulation in CPCs. In contrast, the small conductance calcium-activated potassium channel (K_{Ca}2.3) encoded by the *KCNN3* gene was unchanged. The $\beta 4$ regulatory subunit of the large-conductance calcium-activated potassium channel (*KCNMB4*) was significantly downregulated in CPCs. *KCNB1* (voltage-gated potassium channel subunit Kv2.1); *KCND2* (Kv4.2) and *KCNH6* (Kv11.2) were also downregulated in CPCs (Table S1).

Whilst most of the genes coding for the alpha subunits of voltage-gated sodium channels were upregulated in CPCs, with *SCN2A* encoding the Na_v1.2 sodium channel showing a 1.3-fold upregulation, all epithelial sodium channel subunit genes (*SCNN1A*, *SCNN1B*, *SCNN1D*, *SCNN1G*) were found to show a trend towards downregulation (Table S2), suggesting an altered K⁺/Na⁺ ion handling in CPCs. The only gene showing a significantly lower expression in CPCs was *SCNN1D*. We also checked the expression patterns of genes encoding the alpha and beta subunits of the Na⁺/K⁺-ATPase and found that the *ATP1A1* gene was significantly downregulated in CPCs. Genes coding for the rest of the subunits were unchanged.

Interesting differences were found also in the expression patterns of genes coding for proteins involved in global calcium handling. The genes coding for molecules that regulate store-operated Ca²⁺ entry (SOCE); inositol 1,4,5-trisphosphate receptors (IP₃Rs) that mediate calcium release from the intracellular calcium stores; as well as the sarcoplasmic/endoplasmic reticulum Ca²⁺ ATPase (SERCA) that are responsible for calcium sequestration, were showing a trend for downregulation in CPCs. Transcript levels of

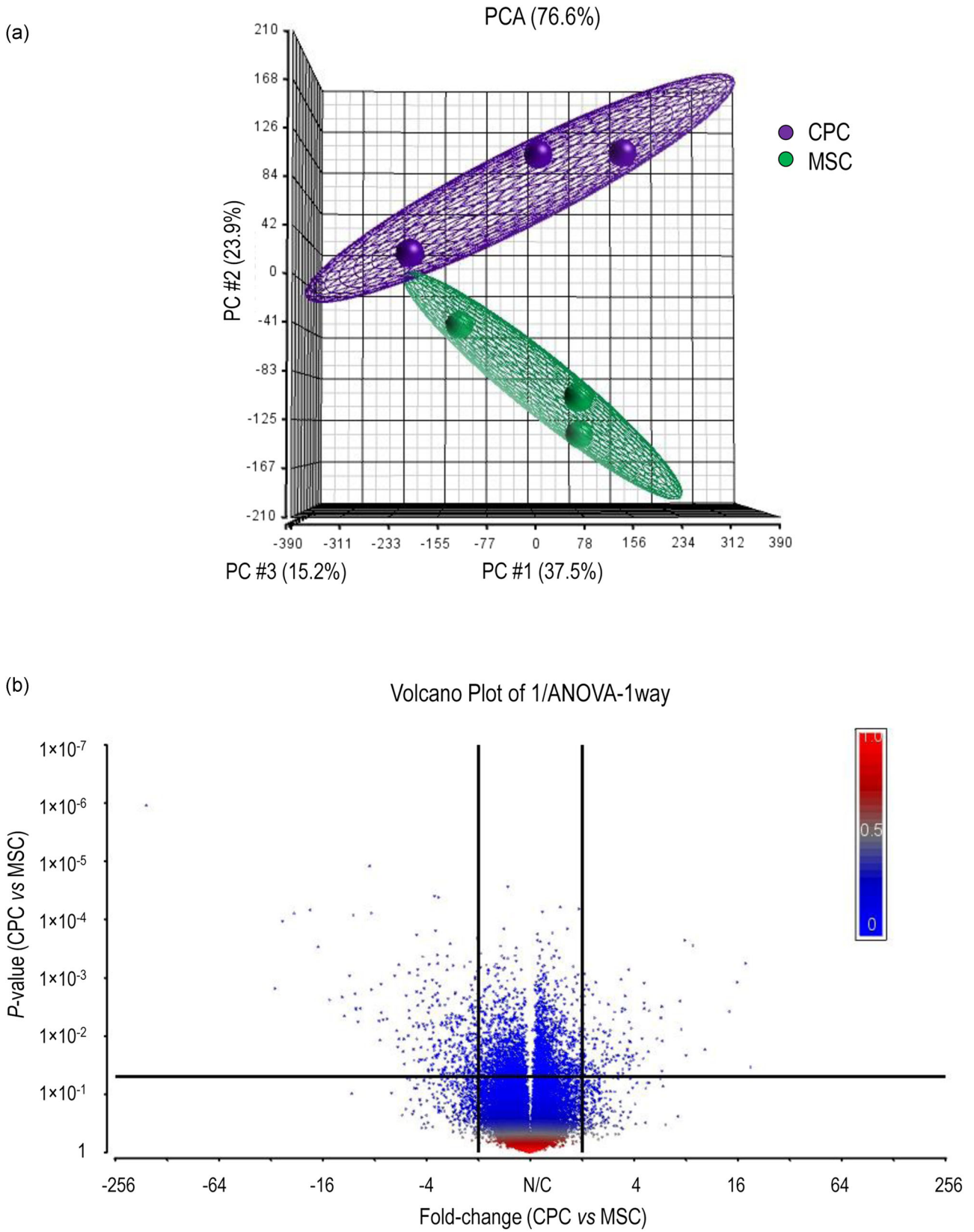


FIGURE 1 (See caption on next page)

both *ORAI2* and *ATP2A3* (*SERCA3*) displayed a significant reduction in CPCs. In contrast, genes coding for voltage-gated calcium channel subunits were unchanged. In a similar way, the ATPases and exchangers that mediate calcium extrusion (*PMCA2-4*, as well as *NCX1-2*); as well as the metabotropic purinergic receptors were also unchanged with a trend towards upregulation, with the exception of *P2RY2*, which was significantly downregulated in CPCs. The genes coding for nonselective cation channels, including members of the ionotropic P2X purinergic receptors, as well as the TRP cation channel families TRPC and TRPV, were showing a general trend towards downregulation, in particular, *TRPC4* and *TRPV2* (Table S3).

We have also looked at other ion channel expression patterns and found that the only gene which had a significantly different expression (downregulation in CPCs) between the two cell types was *ASIC1* coding for the acid-sensitive cation channel subunit 1. None of the other transcripts showed significantly different expression levels between CPCs and MSCs (Table S4).

3.2 | Validating microarray data by RT-qPCR confirmed the differential expression of ion channel genes in CPCs

The messenger RNA (mRNA) expression profiles of selected candidate genes encoding various ion channel subunits were first validated using custom-configured TaqMan 96-Well Fast Gene Expression Array plates (see Tables S5 and S6). Given their role in chondrogenitor and chondrocyte physiology, we were particularly interested in studying the roles of the calcium-activated potassium channels, and therefore we looked at the expression patterns of the genes encoding the various subunits of these channels in details. To confirm the expression patterns of these genes, we employed custom-designed primers and performed individual qPCR reactions. The genes coding for the α and β subunits of the large-conductance calcium-activated potassium channel (BK) were all detected; *KCNMA1* and *KCNMB4* were upregulated; *KCNMB1* was downregulated in CPCs; *KCNMB2* and *KCNMB3* were unchanged. Of the genes encoding the small conductance calcium-activated potassium channel proteins 1–3 (*KCNN1–3*), *KCNN1* was unchanged, whereas *KCNN3* was massively downregulated in CPCs. The gene for the intermediate conductance calcium-activated potassium channel protein 4 (*KCNN4*) was showing a significant downregulation in CPCs (Figure 3). Differences were detected between our qRT-PCR and microarray data. This has been observed before and is largely attributed to the differences in probe sequences (Canales et al., 2006); however, the observed differences

could also be attributable to different methodological aspects of the two approaches, such as the fundamentally different data normalisation strategies (Morey et al., 2006).

3.3 | Modulation of the BK potassium channel alters cell proliferation, marker gene expression and migration of CPCs

To assess the role of large-conductance calcium-activated potassium channels in CPCs and MSCs on cell proliferation and viability (mitochondrial activity), cells were incubated in the presence of the selective BK channel inhibitors IBTX (100 nM) and paxilline (1 μ M); or the BK channel activator NS1619 (10 μ M) before assays. Whilst none of the tested compounds interfered with the mitochondrial activity of the cells (i.e., did not have adverse effects on general cell physiology; Figure 4a), both IBTX and paxilline significantly reduced the proliferation rate in CPCs, but had no significant effect in MSCs (Figures 4b and S2). When CPCs were cultured in the presence of 1 μ M paxilline, the osteogenic transcription factor *RUNX2* was significantly upregulated compared to the control, whereas the expression profile of *SOX9*, the chondrogenic master regulator, remained unchanged. *COL1A1*, on the other hand, was upregulated following paxilline treatment (Figure 4c).

Given that the CPCs employed in this study have previously been demonstrated in vitro and in vivo migratory features (Koelling et al., 2009), we performed two different migration assays with or without the BK channel inhibitor paxilline. Fibronectin-guided migration of CPCs in a Boyden chemotaxis chamber was significantly increased in the presence of 1 μ M paxilline (Figure 5a). The effect of paxilline was also examined in random cell migration assays. Paxilline at 1 μ M enhanced the migratory parameters of chondrogenitor cells, significantly increased the total path of migration, the maximum distance from the origin; furthermore, the average cell speed was also significantly greater compared to the control (Figure 5b). Next, we shifted the migratory tracks (total paths) of the individual cells to a common origin to generate static wind rose plots (Figure 5c). The bigger diameter of the wind rose plot in paxilline-treated cells indicates the increased motility of these cells.

3.4 | Electrophysiological properties and intracellular calcium oscillations of chondrogenitor cells

CPC and MSC cell lines with a characteristic mesenchymal morphology were grown under standard culturing conditions before

FIGURE 1 (a) Principal component analysis (PCA) showing transcriptomic differences between expression microarray data of both chondrogenic progenitor cell (CPC) and mesenchymal stem cell (MSC) ($N = 3$). Each sample group is represented by a sphere and is colour-coded to indicate the corresponding cell type category. There is a clear difference in the transcriptomic clustering between MSC and CPC samples. (b) Volcano plot showing differentially expressed genes between CPC and MSC cells. The vertical axis (y-axis) corresponds to the $\log_{10} p < .05$ and the horizontal axis (x-axis) displays the \log_2 fold change. Based on these parameters, the dots in the upper left and right areas represent differentially expressed genes with statistical significance. ANOVA, analysis of variance

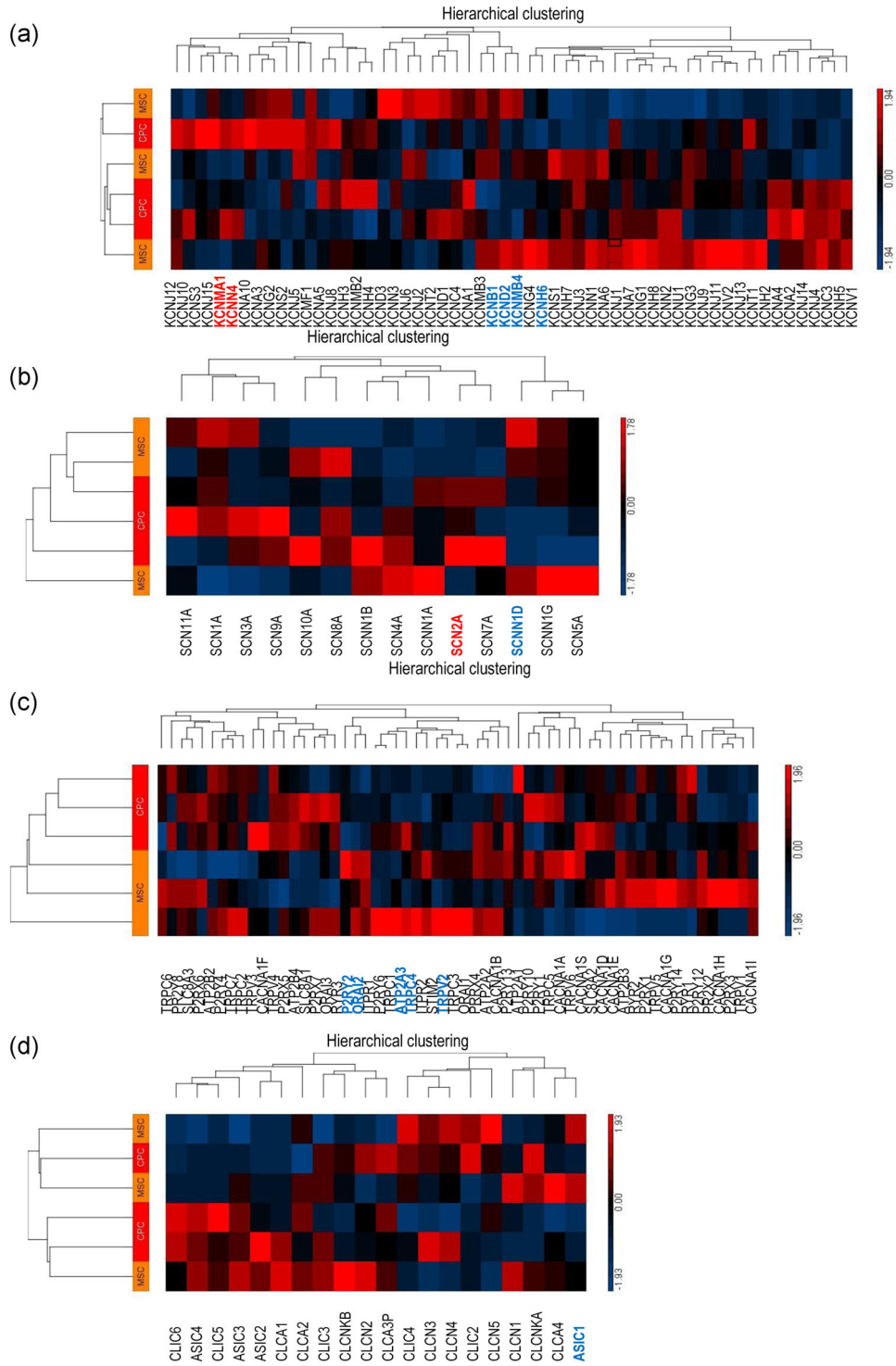


FIGURE 2 Heatmaps and hierarchical clustering dendrograms for genes coding for (a) potassium channel subunits, (b) sodium channel subunits, (c) proteins involved in mediating calcium homeostasis and other nonselective ion channels and (d) acid-sensitive cation channels and chloride channels. Results are expressed as fold change of gene expression of chondrogenic progenitor cell (CPC) versus mesenchymal stem cell (MSC). The red colour represents upregulation, the black colour indicates an unchanged expression, and the blue colour represents the downregulation of expression. The pattern and length of the branches in the dendrogram reflect the relatedness of the samples. Genes that were significantly up- or downregulated in CPC versus MSC cells are highlighted in boldface; the red colour represents upregulation, and the blue colour represents downregulation of expression. N = 3 biological replicates

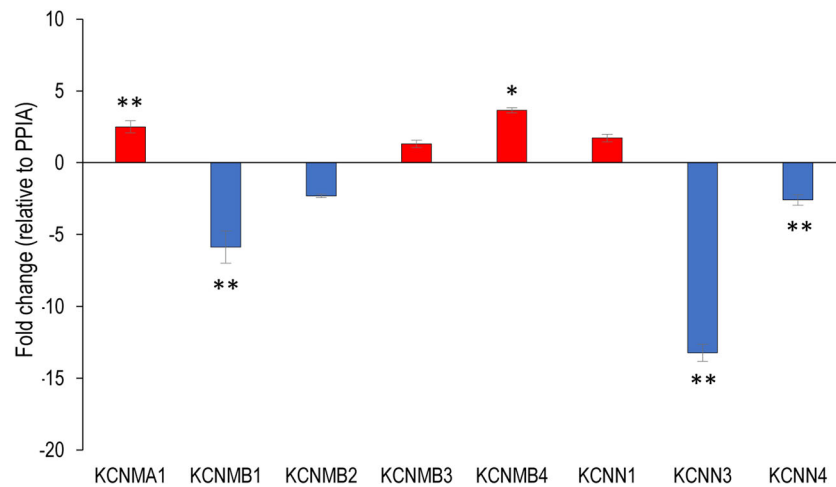


FIGURE 3 Transcript expression levels of selected genes coding for Ca^{2+} -dependent potassium channel subunits as determined by a quantitative real-time polymerase chain reaction in chondrogenic progenitor cells. Red bars represent upregulation, and blue bars represent downregulation of expression relative to mesenchymal stem cells (MSCs), after being normalised to the reference gene *PPIA*. Representative data (average \pm SEM; $N = 3$) out of three independent experiments (biological replicates) showing the same tendency of changes. Statistically significant (* $p < .05$; ** $p < .01$) differences compared to MSCs are marked by an asterisk(s)

preparation for DEP analysis (Figure 6a). The measured DEP spectra of the cell lines were used to determine specific membrane capacitance (C_{Spec}) and conductance (G_{Spec}) values; as these calculations take cell size into account (the values of capacitance and conductance are cell size-independent), the cell radii were determined after trypsinisation, which was statistically different. The electrophysiological properties of CPC and MSC cells are shown in Figure 6b, and summarised in Table 1. Effective membrane capacitance (C_{Eff}) is a measure of the ability of the membrane to store charge and generate a dipole in a frequency-dependent manner in DEP. The C_{Eff} values of CPC and MSC cells were not significantly different from each other. The membrane capacitance per cell area values were also very similar between CPC and MSC. The intracellular conductivities of CPC and MSC were also almost identical between the two cell types. The greatest difference between the two cell types was seen with regard to the specific membrane conductance (G_{Spec}) parameter: CPCs were characterised by a significantly higher G_{Spec} value than MSCs, which equals to a 32.8% difference. Representative DEP spectra for CPC and MSC cells are shown in Figure 6c.

As RT-qPCR analysis revealed changes in the expression of several ion channels at the mRNA level, whole-cell currents were examined. Both CPC and MSC cells were heterogeneous in respect to the ionic current expression. The significant current was recorded in 6 of 27 CPC cells. The voltage-dependent features of these outward currents were reminiscent of that of BK channels. In addition, the time-dependent component was inhibited by paxilline, indicating that the current was partially carried by BK channels. The linear component of the current was not specified further. In a similar way, the paxilline-sensitive composite current was observed in four of seven MSC cells (Figure 7a,b). The RMP of CPCs did not differ significantly from that of MSCs as determined by whole-cell patch-clamp measurements (-24.1 vs. -21.3 mV) (Figure 7c).

Since CPCs have been previously described to display oscillations in cytosolic calcium levels, we also looked at whether paxilline interfered with these spontaneous calcium events. In control cultures, 16% of CPCs exhibited periodic changes in cytosolic Ca^{2+} concentration ($n = 112$), but $1 \mu\text{M}$ paxilline completely abolished such events ($n = 83$) (Figure 7d).

4 | DISCUSSION

OA is a multifaceted and highly heterogeneous whole-joint disease without a common pathophysiological pathway. Therefore, it is unlikely that a single therapeutic target can change the course of disease progression. There are currently no therapeutic strategies able to halt or significantly delay OA progression, and the existing pharmacological treatments are unable to sustain effective and long-lasting symptomatic relief. At present, joint replacement with an artificial prosthesis is the single most effective measure to improve patient quality of life, but of course not all OA patients will progress to this stage (Conaghan et al., 2019). To develop novel therapeutic approaches targeting OA, a more profound understanding of the molecular mechanisms of the disease is required. A broad spectrum of ongoing trials and treatment options target various aspects of the disease, including cartilage and bone regeneration or repair, inflammatory and pain processes, altered metabolic pathways and senescence (Grassel & Muschter, 2020).

Certain stem cell-based cartilage regenerative approaches are already in the phase I clinical study stage. BM-MSCs and adipose tissue-derived MSCs (AD-MSCs) are currently the preferred cell types for regenerative strategies (Grassel & Muschter, 2020). However, whether MSCs are really the optimal cell population for cartilage regenerative therapy is still controversial. In this study, we

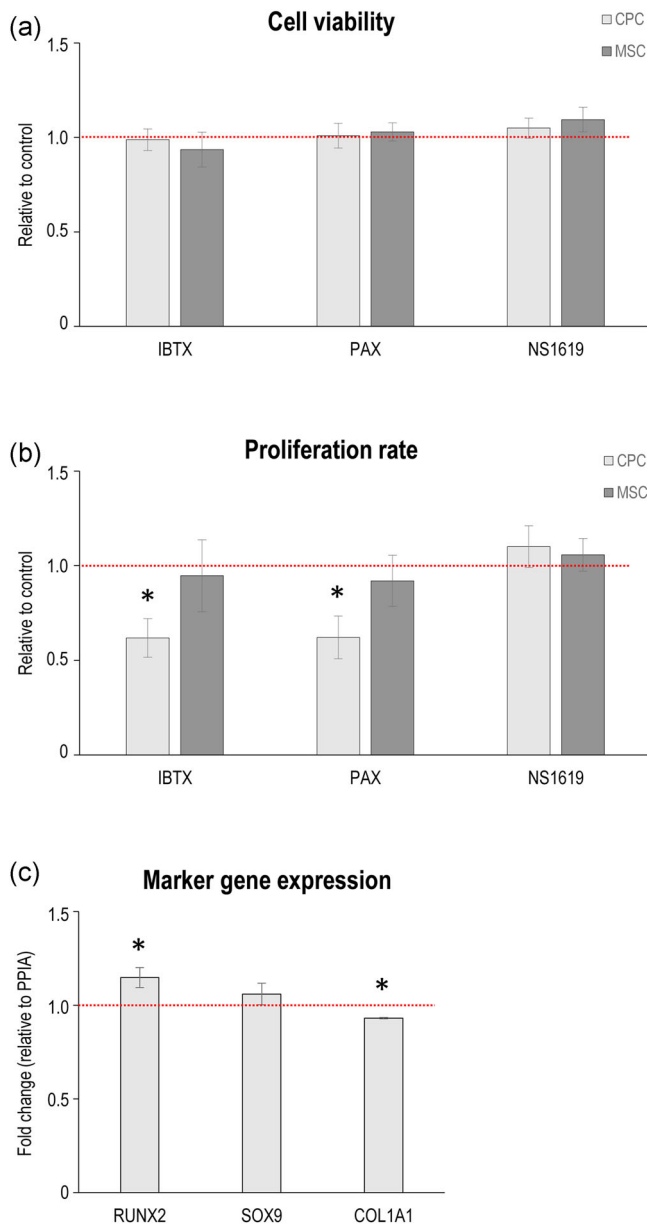


FIGURE 4 Mitochondrial activity, as a measure of cell viability (a) and proliferation rate (b) were determined by 3-(4,5-dimethylthiazol-2-yl)-2,5-diphenyltetrazolium bromide test and ^3H -thymidine incorporation assays, respectively, following pharmacological modulation of BK channel function in chondrogenic progenitor cell (CPC) versus mesenchymal stem cell (MSC). Representative data (average \pm SEM) out of three independent experiments ($N = 3$ biological replicates) showing the same tendency of changes (data are mean of $n = 8$ samples in each replicate). For each experimental group, data were normalised to that of the respective vehicle control (not shown individually). Statistically significant ($*p < .05$) differences compared to the vehicle control are marked by an asterisk. (c) Osteochondrogenic marker gene expression after $1 \mu\text{M}$ paxilline treatment as determined by a quantitative real-time polymerase chain reaction in CPC cells after being normalised to PPIA. Representative data (mean \pm SEM; $n = 3$) out of three independent experiments (biological replicates) showing the same tendency of changes. Statistically significant ($*p < .05$) differences compared to control (dimethyl sulfoxide) CPCs are marked by an asterisk(s)

turned our attention to alternative cell sources with potentially superior chondrogenic potential compared to BM-MSCs, which could be exploited for future cartilage regenerative therapies. Migratory CPCs have been partially characterised; they are known to exhibit a distinct transcriptomic signature compared to osteoblasts, chondrocytes and immortalised foetal chondrocytes (T/C-28 cells) (Koelling et al., 2009). However, the specific cellular identity and detailed molecular phenotype of CPCs is still elusive. Therefore, the aim of this study was to elucidate the biology and phenotype of CPCs by comparing their transcriptomic profile with BM-MSCs. Given the unique ionic composition of the CPC niche within the ECM of diseased cartilage, we were especially interested in differences in the channelome of CPCs, focusing on K^+ and Ca^{2+} transporters potentially involved in maintaining the progenitor phenotype under inflammatory conditions. We also mapped the electrophysiological profile of CPCs using patch-clamp and DEP.

We have recently analysed the surfaceome of CPCs using selective cell surface protein labelling followed by high-throughput mass spectrometry and identified alterations in the composition of the surfaceome compared to BM-MSCs (Matta et al., 2019). However, even the high-throughput mass spectrometry-based approach that we employed was not sensitive enough to detect alterations in very low-abundance ion channels and transporters. Here, we performed microarray analysis and compared the global gene expression signatures of CPCs to BM-MSCs. CPCs harboured a distinct transcriptomic profile and mRNA expression pattern that was different to that of MSCs. Pathway analysis confirmed that mainly cell cycle-related and DNA/nucleic acid metabolism-related GO categories were overrepresented in the list of genes with significantly different expression levels, which was clearly reflected by the lower proliferation rate of CPCs compared to MSCs. There was a 64% correlation with the direction of fold changes of differentially expressed transporter genes when we compared their pattern to the data generated by quantitative mass spectrometric analysis on the surfaceome of CPC and MSC cells (Table S8; see also File S2) (Matta et al., 2019).

4.1 | Differential K^+ transporter gene expression profiles in CPCs

We chose to study the expression profiles of those ion channels and transporter families that may have relevance in chondroprogenitor cell physiology (Barrett-Jolley et al., 2010; Matta & Zakany, 2013; Mobasheri et al., 2019). The most widely reported ion channels in chondrocytes and MSCs are potassium channels (Mobasheri et al., 2012; Pchelintseva & Djamgoz, 2018). The human genome contains around 70 different potassium channel genes, which makes them the largest family of membrane ion channels (Mobasheri et al., 2012). The α -subunit (KCNMA1) of the large-conductance Ca^{2+} -activated potassium channel (BK, BK_{Ca} , MaxiK), as well as the intermediate Ca^{2+} -activated potassium channel (IK, KCNN4, SK4,

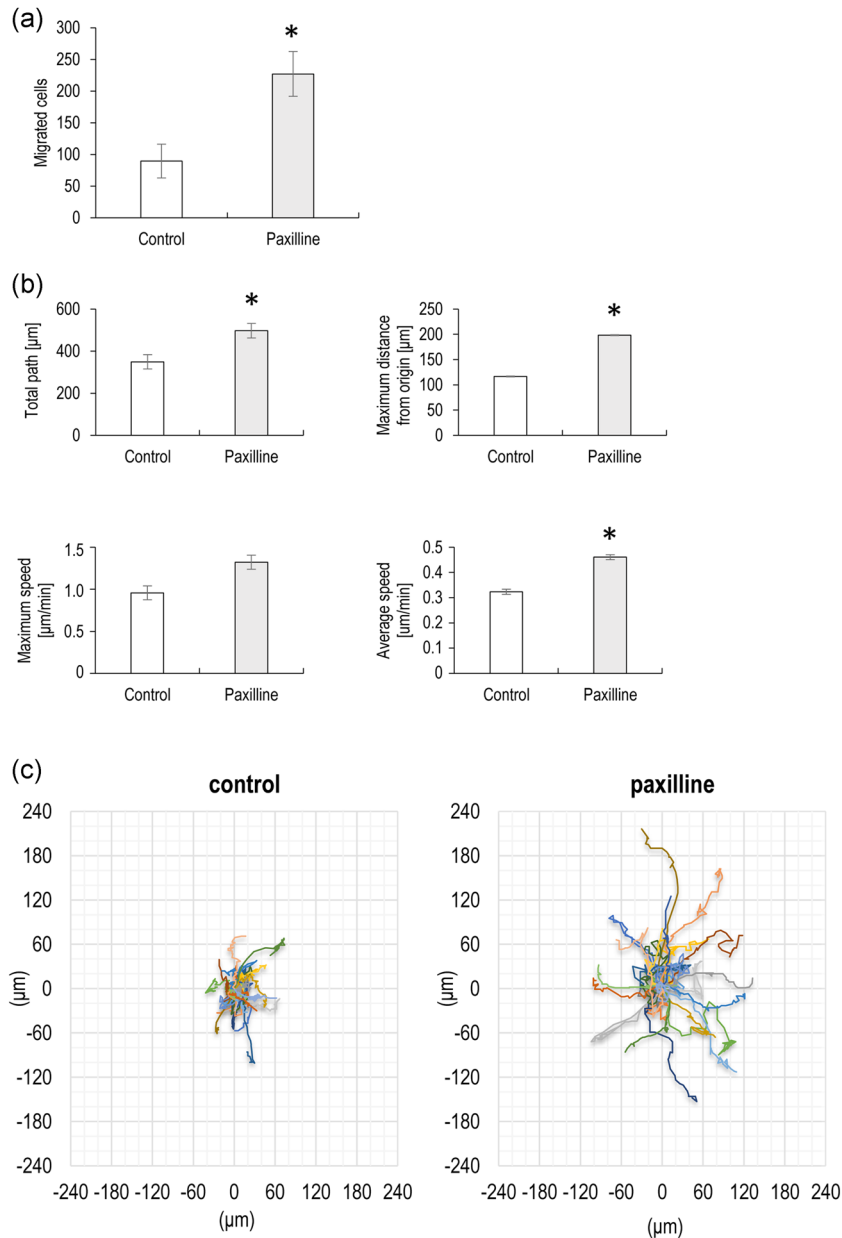


FIGURE 5 (a) Fibronectin-guided migration of chondrogenic progenitor cells in a Boyden chemotaxis chamber was significantly increased in the presence of $1\ \mu\text{M}$ paxilline. Data shown are mean \pm SEM; * $p < .05$. $N = 3$ independent experiments. (b) The total length of movement, the maximum distance from the starting point, the average cell speed, and the maximum speed of the chondroprogenitor cells are depicted either without or with $1\ \mu\text{M}$ paxilline treatment as determined during live-cell imaging. The total duration of live-cell microscopy was 18 h; frame rate: 2/1 h; $N = 3$ independent experiments; 24–27 cells were analysed in each experiment. Total number of analysed cells: 77–80 cells/treatment group. Data are reported as mean \pm SEM; * $p < .05$. (c) Representative wind-rose plots depict the total path of the cells. Each coloured line represents the total path of a single chondroprogenitor cell either without or with $1\ \mu\text{M}$ paxilline treatment

$K_{Ca}3.1$) transcripts, displayed the largest fold changes, with a 50% upregulation in CPCs. BK channels have been detected in undifferentiated MSCs both at the mRNA level and by single-channel recordings (Kawano et al., 2003), and also in mature chondrocytes (Mobasheri et al., 2010). BK channels may play various roles in chondrocyte physiology including volume regulation, oxygen sensing and mechanotransduction (Mobasheri et al., 2012). Since BK channels have been implicated in driving MSC differentiation (Pchelintseva & Djamgoz, 2018), perhaps the fact that CPCs are more committed to the chondrogenic lineage than undifferentiated MSCs may explain the higher levels of *KCNMA1* both at the transcript and at the protein level (Matta et al., 2019).

BK channels may also be potential drug targets to protect against joint degeneration in OA (Haidar et al., 2020). In an in vitro model of synovial inflammation, *KCNMA1* was found to be upregulated following

cytokine treatment in primary synovial fibroblasts (Haidar et al., 2020). BK channel expression was also found to be upregulated in human OA cartilage (Lewis et al., 2013). Given that the migratory CPCs used in this study had been isolated from late-stage OA, the increased *KCNMA1* expression may also be a result of their original inflammatory niche.

To further characterise the contribution of BK channels to the chondroprogenitor phenotype, we first looked at whether BK channel function was required for cell division. The role of BK channels in mediating proliferation has been controversial. BK channels are known to stimulate proliferation in BM-MSCs (Zhang et al., 2014); however, their activation may also lead to antiproliferative effects in human-induced pluripotent stem cell-derived MSCs (Zhao et al., 2013). The BK channel inhibitors paxilline and IBTX have significantly lowered the proliferation rate of CPCs, but not in MSCs. This may be attributed to the different sensitivity of the two cell

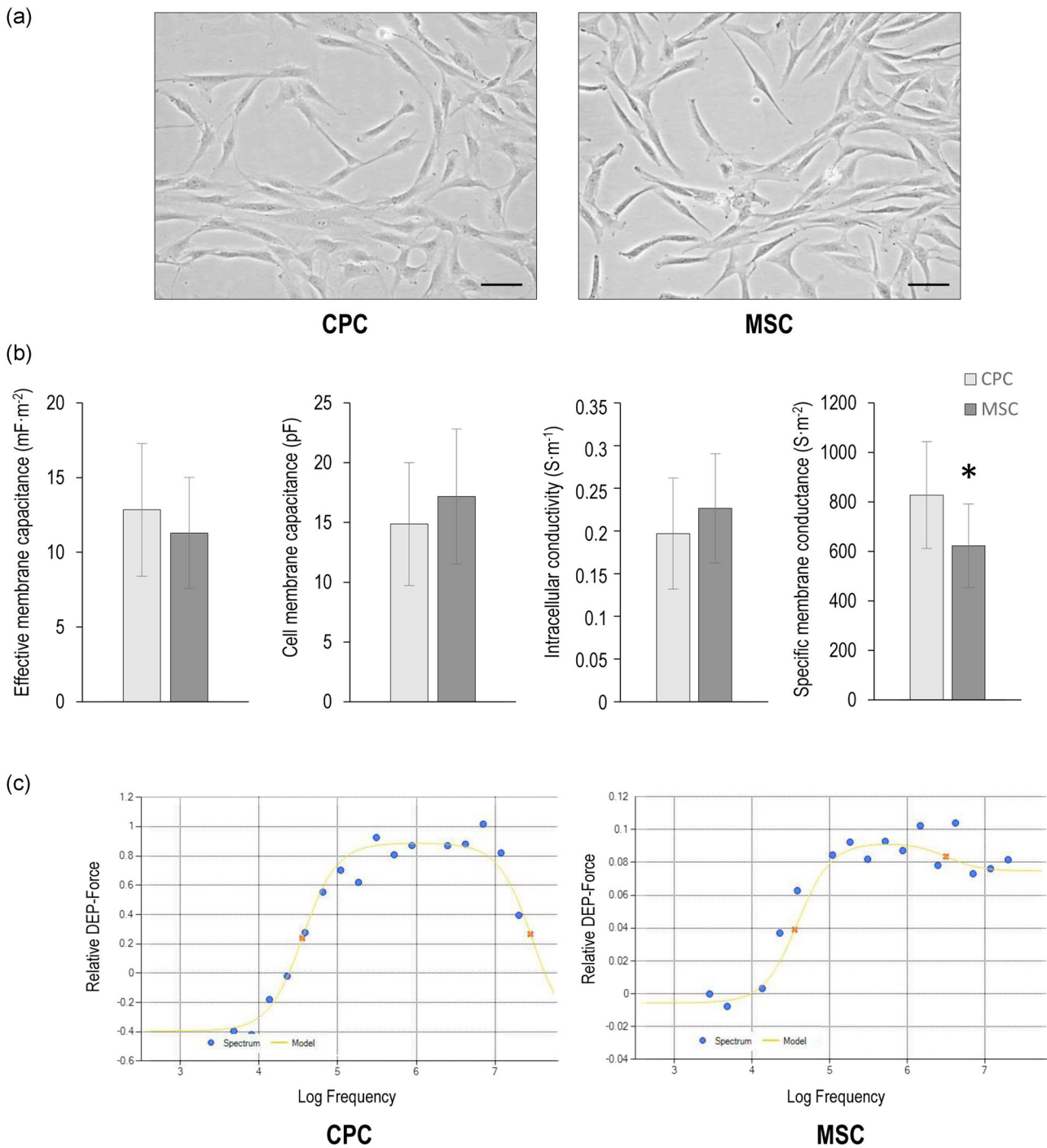


FIGURE 6 (a) Representative photomicrographs of chondrogenic progenitor cell (CPC) and mesenchymal stem cell (MSC) morphology before preparations for dielectrophoresis (DEP) measurements, showing typical mesenchymal cell morphology. Scale bar = 30 μm . (b) DEP parameters of CPCs and MSCs. The effective membrane capacitance (C_{Eff}), intracellular conductivity and specific membrane conductance (G_{Spec}) values were derived by fitting lines of best fit to DEP spectra and applying the 'single-shell model'. Membrane capacitance per cell was calculated by multiplying the capacitance values with the average surface area of the cells. Error bars denote the SD. Each experiment was repeated three times ($N = 3$). Asterisk denotes a statistically significant difference ($*p < .05$). (c) Examples of typical electrophysiological DEP (light intensity) spectra of CPCs ($n = 22$) and MSCs ($n = 14$) produced using the DEP-microwell, together with a 'best-fit' model from which the dielectric properties were determined. Changes in light intensity in the region of interest detected over a 30 s exposure were plotted against frequency (between 1.6 kHz and 20 MHz). The spectra are negative at low frequencies, where cells are repelled from the electrodes; at higher frequencies, the spectra become positive, where cells are being attracted to the electrodes. The spectra gradually increase until a plateau stage is reached. At even higher frequencies, the spectra begin to decrease (mainly for CPCs)

	CPC	MSC	p Value
Cell radius (μm)	9.6 (± 1.43)	11 (± 1.37)	<.001
Effective membrane capacitance (mF/m^2)	12.84 (± 4.44)	11.29 (± 3.71)	.298
Membrane capacitance per cell (pF)	14.86 (± 5.13)	17.16 (± 5.65)	.231
Intracellular conductivity (S/m)	0.19 (± 0.06)	0.22 (± 0.06)	.203
Specific membrane conductance (S/m^2)	827.48 (± 215.64)	623.15 (± 168.56)	.006

Note: Values shown were averaged over three repeats of separate populations with \pm SD given in brackets.

Abbreviations: CPC, chondrogenic progenitor cell; DEP, dielectrophoresis; MSC, mesenchymal stem cell.

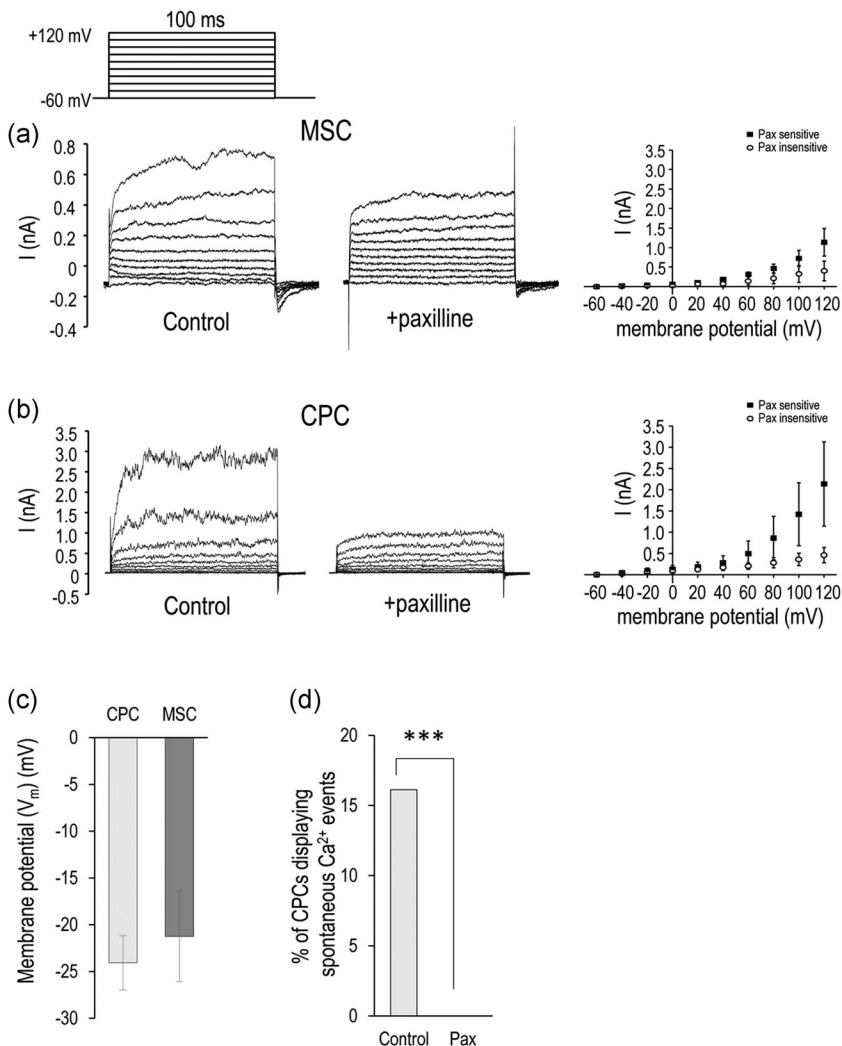


TABLE 1 Electrophysiological characteristics of CPC and MSC cells grown in standard monolayer cultures as determined by the DEP well chip and the single-shell model applied to the data

FIGURE 7 Representative whole-cell currents of mesenchymal stem cell (MSC) and chondrogenic progenitor cell (CPC). Resting membrane potential was held at -60 mV. Current elicited by voltage step depolarizations between -40 and $+120$ mV are shown in MSC (a) and CPC (b) cells under control conditions and during paxilline treatment ($n = 27$ for CPC and 7 for MSC). For both (a) and (b), I-V relationship of outward, paxillin-sensitive (full squares) and paxillin-insensitive (empty circles) currents in MSC ($n = 7$) and CPC ($n = 27$) cells are also shown. (c) Resting membrane potential values determined during patch-clamp measurements ($n = 22$ for CPC and 8 for MSC). (d) Spontaneous calcium events in CPCs determined during live-cell Ca^{2+} imaging ($n = 112$ control vs. 83 paxilline-treated). Asterisks denote a statistically significant difference ($***p < .001$). Pax, paxilline

types to BK channel inhibition, and the dose-dependent effect of paxilline on proliferation. Whilst $1 \mu\text{M}$ paxilline caused approximately 10% reduction in DNA synthesis in BM-MSCs, at $3 \mu\text{M}$ it resulted in approximately 80% inhibition (Zhang et al., 2014). On the other hand, in line with our data, IBTX did not alter $[\text{H}^3]$ -thymidine incorporation levels in rat BM-MSCs (Deng et al., 2007).

The increased abundance of *KCNN4* transcripts in CPCs may reflect their inherently enhanced cell motility as IK channels have a confirmed

role in migration (Pchelintseva & Djamgoz, 2018). In contrast, BK channels have a rather controversial role in cell motility (Catacuzzeno et al., 2015). In migratory CPCs, BK channels may play an inhibitory role in the motility of the cells as paxilline treatment increased every parameter of migration. These findings are rather unexpected as the BK channel inhibitor IBTX was reported to block the platelet lysate-induced migration of MSCs (Echeverry et al., 2020). In glioma cells, however, BK channel openers inhibited migration (Kraft et al., 2003). Given that CPCs

express both *SOX9* and *RUNX2* and that there is a degree of crosstalk between these transcription factors (Koelling et al., 2009), perhaps BK blockade influenced CPC behaviour in such a way that it attenuated their chondrogenic phenotype, which is also reflected in the upregulation of the osteogenic transcription factor *RUNX2*.

4.2 | Ca^{2+} homeostasis in chondroprogenitor cells

Given that BK channel function depends on both RMP and $[\text{Ca}^{2+}]_i$, we undertook to look at the transporters mediating the Ca^{2+} homeostasis of the chondroprogenitor cells. Calcium plays central roles in cell physiology in nonexcitable cells such as chondrocytes (Suzuki et al., 2020). Dynamic changes in calcium signalling have been shown to be paramount to chondrogenesis (Matta & Zakany, 2013), and we have described earlier the calcium handling in CPCs (Matta et al., 2015). SOCE, one of the main sources of Ca^{2+} influx, is mediated by Ca^{2+} release-activated Ca^{2+} channels formed of ORAI1, ORAI2 and ORAI3 proteins. We found that ORAI2 was present in lower abundance in CPCs; ORAI2 has been reported to modulate the magnitude of SOCE (Inayama et al., 2015; Vaeth et al., 2017), which further pinpoints the important role of SOCE in CPC homeostasis. Given that purinergic signalling regulates intracellular Ca^{2+} oscillations in CPCs and MSCs (Jiang et al., 2017; Matta et al., 2015), we also looked at differences in purinergic receptor transcript levels. The only gene with a significantly altered expression was *P2RY2*, which codes for a metabotropic receptor involved in the negative regulation of the osteogenic differentiation of BM-MSCs (Li et al., 2016).

BK channel function was reported to modulate $[\text{Ca}^{2+}]_i$ oscillations in various cell types (Mizutani et al., 2016; Wakle-Prabakaran et al., 2016). Both CPCs (Matta et al., 2015) and MSCs (Kawano et al., 2003) are known to exhibit periodic fluctuations in resting cytosolic Ca^{2+} levels. We confirmed that BK channels play a central role in mediating the Ca^{2+} homeostasis in CPCs since the BK channel inhibitor paxilline completely abolished these $[\text{Ca}^{2+}]_i$ oscillations. This is the first study to report a mechanistic link between the big conductance calcium-sensitive potassium channels and periodic $[\text{Ca}^{2+}]_i$ oscillations in chondroprogenitor cells.

4.3 | Electrophysiological profiling of CPCs

Having established the channelome of CPCs at the transcript level, we then looked at whether the global electrophysiological profile (electrome) of the progenitor cells was different from that of BM-MSCs. In addition to conventional patch clamping, we also employed DEP, which has been shown to be an efficient quantitative method of differentiating between closely related cell types, for example, in the bone marrow (Ismail et al., 2015). DEP can be used for both assessing the passive electrical properties of cellular components and as the basis for a separation method (Mahabadi et al., 2018). This could be especially relevant for CPCs present at very low abundance in arthritic cartilage, given that a truly reliable cell surface marker has still not been identified. Inherent cell properties that do not require the use of specific labelling

for detection would provide a unique means to identify progenitors committed to particular cell fates. Whilst the effective membrane capacitance and the intracellular conductivity values did not differ, we report membrane conductance as a specific electrophysiological property that reflects the differentiation stage of human CPCs and MSCs. Membrane conductivity is a parameter that describes the potential of the membrane to transmit charge; and is indicative of ionic flux (Henslee et al., 2017).

We employed patch clamping to establish the RMP of CPCs, which was not statistically different from that of MSCs. The V_m value of MSCs detected in our study (approximately -20 mV) was similar to what has been observed earlier (-10 mV) (Kawano et al., 2003). The RMP of mature chondrocytes is dependent on the coordinated function of different types of ion channels including nonselective cation channels (Lewis et al., 2011) and K^+ channels (Maleckar et al., 2018; Wilson et al., 2004). The majority of these channels did not show statistically different expression between MSCs and CPCs, which probably explains why there is no difference in RMP as observed in this study. As described above, various K^+ channels were detected at the transcript level in both cell types; therefore, we studied the outward whole-cell currents in CPC and MSC cells. Both cell populations were heterogeneous with respect to ion current expression, and we found evidence of paxilline-sensitive conductances.

5 | SUMMARY AND CONCLUSIONS

Here we have provided evidence, for the first time, that BK channels were functional in undifferentiated CPCs, as the voltage-dependent features of the detected potassium currents were reminiscent of that of BK channels. In addition, the time-dependent component was inhibited by paxilline, indicating that the current was partially carried by BK channels. Functional BK channels were required for maintaining the balanced differentiation state of CPCs as paxilline treatment significantly upregulated the osteogenic transcription factor *RUNX2*, which favours osteogenic differentiation potentials.

In line with our previous paper describing the Ca^{2+} homeostasis of CPCs (Matta et al., 2015), here we provide experimental data supporting the hypothesis that periodic increases in $[\text{Ca}^{2+}]_i$ may activate BK channels. The ionic fluxes mediated by these channels may alter the RMP, which in turn modulates Ca^{2+} influx. Such a feedback loop has been recently proposed to exist in chondrocytes (Suzuki et al., 2020); we have now identified the key components of that loop in CPCs in this study. It is plausible to hypothesise that under resting conditions, the $[\text{Ca}^{2+}]_i$ peaks could activate BK channels to such an extent that the K^+ efflux they mediate does not favour the changes in cell volume and shape required for cell migration.

6 | PERSPECTIVES

A recent systematic review has analysed the outcome of 17 studies assessing articular cartilage repair after the clinical application of cell populations containing MSCs in human subjects with knee OA

(Ha et al., 2019). Significantly better clinical outcomes (improvement of the cartilage state on magnetic resonance imaging or repaired tissue on second-look arthroscopy) were reported in the MSC group in most of the studies. However, there is limited evidence to support the efficacy of intra-articular MSC-based therapy. This highlights opportunities for identifying alternative cell sources. Whilst the preferred cells used were bone, adipose tissue or umbilical cord-derived MSCs, perhaps exploiting the resident cartilage progenitor cell population present in both healthy and OA cartilage may further enhance the efficacy of such novel therapies. We demonstrate here that CPCs are a distinct cell population but are still similar to BM-MSCs in many ways. This study adds key mechanistic and cellular phenotype data to the in-depth characterisation of cartilage progenitor cells; however, further research is necessary to reconstruct the progenitor niche which would promote their hyaline cartilage regenerative potential.

ACKNOWLEDGEMENTS

The authors are thankful to Krisztina Biróné Barna for skilful technical assistance. The authors would also like to acknowledge the contribution of William Kothalawala Jayasekara and Roland Ádám Takács. Csaba Matta was supported by the European Commission through a Marie Skłodowska-Curie Intra-European Fellowship for career development (Project no. 625746; acronym: CHONDRION; FP7-PEOPLE-2013-IEF), the Premium Postdoctoral Research Fellowship of the Eötvös Loránd Research Network (ELKH) and the Young Researcher Excellence Programme (Grant no. FK 134304) of the National Research, Development and Innovation Office, Hungary. Project no. TKP2020-NKA-04 has been implemented with the support provided by the National Research, Development and Innovation Fund of Hungary, financed under the 2020-4.1.1-TKP2020 funding scheme. Ali Mobasher was the coordinator of the D-BOARD Consortium funded by European Commission Framework 7 programme (EU FP7; HEALTH.2012.2.4.5-2; Project no. 305815; Novel Diagnostics and Biomarkers for Early Identification of Chronic Inflammatory Joint Diseases). Ali Mobasher has received funding from the Deanship of Scientific Research (DSR), King AbdulAziz University (Grant no. 1-141/1434 HiCi). Ali Mobasher is a member of the Arthritis Research UK Centre for Sport, Exercise and Osteoarthritis, funded by Arthritis Research UK (Grant Reference no. 20194). Ali Mobasher wishes to acknowledge financial support from the European Structural and Social Funds (ES Struktūrinės Paramos) through the Research Council of Lithuania (Lietuvos Mokslo Taryba) according to the activity 'Improvement of researchers' qualification by implementing world-class R&D projects' of Measure no. 09.3.3-LMT-K-712 (Grant application code: 09.3.3-LMT-K-712-01-0157; Agreement no. DOTSUT-215) and the new funding programme: Attracting Foreign Researchers for Research Implementation (2018–2022), Grant no. 01.2.2-LMT-K-718-02-0022. Aniko Keller-Pinter was supported by the National Research, Development and Innovation Office of Hungary (Grant no. FK 134684), and by the GINOP-2.3.2-15-2016-00040 project.

CONFLICT OF INTERESTS

The authors declare that there are no conflict of interests.

AUTHOR CONTRIBUTIONS

Conceptualisation: Csaba Matta and Ali Mobasher. *Methodology:* Csaba Matta, Rebecca Lewis, Christopher Fellows, Janos Almassy, Sean May, Peter Szentesi, Aniko Keller-Pinter, Michael P. Hughes and Ali Mobasher. *Software:* Marcos C. Uribe, Szilard Poliska, Janos Fodor, Aniko Keller-Pinter, Fatima H. Labeed and Michael P. Hughes. *Validation:* Csaba Matta, Christopher Fellows and Szilard Poliska. *Formal analysis:* Csaba Matta, Rebecca Lewis, Christopher Fellows, Erin Henslee, Janos Fodor, Janos Almassy and Fatima H. Labeed. *Investigation:* Csaba Matta, Rebecca Lewis, Christopher Fellows, Gyula Diszhazi, Marcos C. Uribe, Szilard Poliska, Peter Szentesi, Tibor Hajdú and Erin Henslee. *Resources:* Janos Almassy, Sean May, James Dixon, Nicolai Miosge, Richard Barrett-Jolley, Peter Szentesi, Aniko Keller-Pinter, Michael P. Hughes and Ali Mobasher. *Data curation:* Csaba Matta, Rebecca Lewis, Christopher Fellows, Janos Almassy, Janos Fodor, Tibor Hajdú, Marcos C. Uribe and Erin Henslee. *Writing - original draft preparation:* Csaba Matta and Rebecca Lewis. *Writing - review and editing:* All authors. *Visualisation:* Csaba Matta, Marcos C. Uribe, Gyula Diszhazi, Szilard Poliska, Janos Fodor, Aniko Keller-Pinter and Erin Henslee. *Supervision:* Nicolai Miosge, Richard Barrett-Jolley, Fatima H. Labeed, James Dixon, Sean May, Peter Szentesi, Aniko Keller-Pinter and Ali Mobasher. *Project administration:* Csaba Matta and Ali Mobasher. *Funding acquisition:* Csaba Matta and Ali Mobasher.

ORCID

Csaba Matta  <http://orcid.org/0000-0002-9678-7420>
 Rebecca Lewis  <http://orcid.org/0000-0003-1395-3276>
 James Dixon  <http://orcid.org/0000-0003-1225-3825>
 Marcos C. Uribe  <http://orcid.org/0000-0002-4682-3008>
 Sean May  <http://orcid.org/0000-0001-5282-3250>
 Szilard Poliska  <http://orcid.org/0000-0002-9722-251X>
 Richard Barrett-Jolley  <http://orcid.org/0000-0003-0449-9972>
 Peter Szentesi  <http://orcid.org/0000-0003-2621-2282>
 Aniko Keller-Pinter  <http://orcid.org/0000-0002-4105-8458>
 Fatima H. Labeed  <http://orcid.org/0000-0002-0092-257X>
 Michael P. Hughes  <http://orcid.org/0000-0001-7385-5876>
 Ali Mobasher  <http://orcid.org/0000-0001-6261-1286>

REFERENCES

- Al Maini, M., Al Weshahi, Y., Foster, H. E., Chehade, M. J., Gabriel, S. E., Saleh, J. A., Al Wahshi, H., Bijlsma, J. W. J., Cutolo, M., Lakhanpal, S., Venkatramana, M., Pineda, C., & Woolf, A. D. (2020). A global perspective on the challenges and opportunities in learning about rheumatic and musculoskeletal diseases in undergraduate medical education: White paper by the World Forum on Rheumatic and Musculoskeletal Diseases (WFRMD). *Clinical Rheumatology*, 39(3), 627–642. <https://doi.org/10.1007/s10067-019-04544-y>
- Almassy, J., & Begenisich, T. (2012). The LRRc26 protein selectively alters the efficacy of BK channel activators. *Molecular Pharmacology*, 81(1), 21–30. <https://doi.org/10.1124/mol.111.075234>

- Andersen, C. L., Jensen, J. L., & Orntoft, T. F. (2004). Normalization of real-time quantitative reverse transcription-PCR data: A model-based variance estimation approach to identify genes suited for normalization, applied to bladder and colon cancer data sets. *Cancer Research*, 64(15), 5245–5250. <https://doi.org/10.1158/0008-5472.CAN-04-0496>
- Archer, C. W., & Francis-West, P. (2003). The chondrocyte. *International Journal of Biochemistry and Cell Biology*, 35(4), 401–404. [https://doi.org/10.1016/s1357-2725\(02\)00301-1](https://doi.org/10.1016/s1357-2725(02)00301-1)
- Asmar, A., Barrett-Jolley, R., Werner, A., Kelly, R., Jr, & Stacey, M. (2016). Membrane channel gene expression in human costal and articular chondrocytes. *Organogenesis*, 12(2), 94–107. <https://doi.org/10.1080/15476278.2016.1181238>
- Barrett-Jolley, R., Lewis, R., Fallman, R., & Mobasher, A. (2010). The emerging chondrocyte channelome. *Frontiers in Physiology*, 1, 135. <https://doi.org/10.3389/fphys.2010.00135>
- Barry, P. H., & Lynch, J. W. (1991). Liquid junction potentials and small cell effects in patch-clamp analysis. *Journal of Membrane Biology*, 121(2), 101–117. <https://doi.org/10.1007/BF01870526>
- Broche, L. M., Labeed, F. H., & Hughes, M. P. (2005). Extraction of dielectric properties of multiple populations from dielectrophoretic collection spectrum data. *Physics in Medicine and Biology*, 50(10), 2267–2274. <https://doi.org/10.1088/0031-9155/50/10/006>
- Buckwalter, J. A., Mankin, H. J., & Grodzinsky, A. J. (2005). Articular cartilage and osteoarthritis. *Instructional Course Lectures*, 54, 465–480.
- Canales, R. D., Luo, Y., Willey, J. C., Austermler, B., Barbacioru, C. C., Boysen, C., Hunkapiller, K., Jensen, R. V., Knight, C. R., Lee, K. Y., Ma, Y., Maqsoodi, B., Papallo, A., Peters, E. H., Poulter, K., Ruppel, P. L., Samaha, R. R., Shi, L., Yang, W., ... Goodsaid, F. M. (2006). Evaluation of DNA microarray results with quantitative gene expression platforms. *Nature Biotechnology*, 24(9), 1115–1122. <https://doi.org/10.1038/nbt1236>
- Catacuzzeno, L., Caramia, M., Sforza, L., Belia, S., Guglielmi, L., D'Adamo, M. C., Pessia, M., & Franciolini, F. (2015). Reconciling the discrepancies on the involvement of large-conductance Ca²⁺-activated K channels in glioblastoma cell migration. *Frontiers in Cellular Neuroscience*, 9, 152. <https://doi.org/10.3389/fncel.2015.00152>
- Conaghan, P. G., Cook, A. D., Hamilton, J. A., & Tak, P. P. (2019). Therapeutic options for targeting inflammatory osteoarthritis pain. *Nature Reviews Rheumatology*, 15(6), 355–363. <https://doi.org/10.1038/s41584-019-0221-y>
- De Loof, A. (2016). The cell's self-generated "electrome": The biophysical essence of the immaterial dimension of life? *Communicative & Integrative Biology*, 9(5), e1197446. <https://doi.org/10.1080/19420889.2016.1197446>
- Deng, X. L., Lau, C. P., Lai, K., Cheung, K. F., Lau, G. K., & Li, G. R. (2007). Cell cycle-dependent expression of potassium channels and cell proliferation in rat mesenchymal stem cells from bone marrow. *Cell Proliferation*, 40(5), 656–670. <https://doi.org/10.1111/j.1365-2184.2007.00458.x>
- Dowthwaite, G. P., Bishop, J. C., Redman, S. N., Khan, I. M., Rooney, P., Evans, D. J., Haughton, L., Bayram, Z., Boyer, S., Thomson, B., Wolfe, M. S., & Archer, C. W. (2004). The surface of articular cartilage contains a progenitor cell population. *Journal of Cell Science*, 117(Pt 6), 889–897. <https://doi.org/10.1242/jcs.00912>
- Echeverry, S., Grismaldo, A., Sanchez, C., Sierra, C., Henao, J. C., Granados, S. T., Sutachan, J. J., & Torres, Y. P. (2020). Activation of BK channel contributes to PL-induced mesenchymal stem cell migration. *Frontiers in Physiology*, 11, 210. <https://doi.org/10.3389/fphys.2020.00210>
- Fellows, C. R., Williams, R., Davies, I. R., Gohil, K., Baird, D. M., Fairclough, J., Rooney, P., Archer, C. W., & Khan, I. M. (2017). Characterisation of a divergent progenitor cell sub-populations in human osteoarthritic cartilage: The role of telomere erosion and replicative senescence. *Scientific Reports*, 7, 41421. <https://doi.org/10.1038/srep41421>
- Gomoll, A. H., & Minas, T. (2014). The quality of healing: articular cartilage. *Wound Repair and Regeneration*, 22(Suppl 1), 30–38. <https://doi.org/10.1111/wrr.12166>
- Grassel, S., & Muschter, D. (2020). Recent advances in the treatment of osteoarthritis. *F1000Research*, 9, 325. <https://doi.org/10.12688/f1000research.22115.1>
- Ha, C. W., Park, Y. B., Kim, S. H., & Lee, H. J. (2019). Intra-articular mesenchymal stem cells in osteoarthritis of the knee: A systematic review of clinical outcomes and evidence of cartilage repair. *Arthroscopy*, 35(1), 277–288. <https://doi.org/10.1016/j.arthro.2018.07.028>
- Haidar, O., O'Neill, N., Staunton, C. A., Bavan, S., O'Brien, F., Zougari, S., Sharif, U., Mobasher, A., Kumagai, K., & Barrett-Jolley, R. (2020). Pro-inflammatory cytokines drive deregulation of potassium channel expression in primary synovial fibroblasts. *Frontiers in Physiology*, 11, 226. <https://doi.org/10.3389/fphys.2020.00226>
- Hdud, I. M., Mobasher, A., & Loughna, P. T. (2014). Effect of osmotic stress on the expression of TRPV4 and BKCa channels and possible interaction with ERK1/2 and p38 in cultured equine chondrocytes. *American Journal of Physiology: Cell Physiology*, 306(11), C1050–C1057. <https://doi.org/10.1152/ajpcell.00287.2013>
- Henrotin, Y., Sanchez, C., Bay-Jensen, A. C., & Mobasher, A. (2016). Osteoarthritis biomarkers derived from cartilage extracellular matrix: Current status and future perspectives. *Ann Phys Rehabil Med*, 59(3), 145–148. <https://doi.org/10.1016/j.jrehab.2016.03.004>
- Henslee, E. A., Crosby, P., Kitcatt, S. J., Parry, J. S. W., Bernardini, A., Abdallat, R. G., Braun, G., Fatoyinbo, H. O., Harrison, E. J., Edgar, R. S., Hoettges, K. F., Reddy, A. B., Jabr, R. I., von Schantz, M., O'Neill, J. S., & Labeed, F. H. (2017). Rhythmic potassium transport regulates the circadian clock in human red blood cells. *Nature Communications*, 8(1), 1978. <https://doi.org/10.1038/s41467-017-02161-4>
- Hoettges, K. F., Henslee, E. A., Torcal Serrano, R. M., Jabr, R. I., Abdallat, R. G., Beale, A. D., Waheed, A., Camelliti, P., Fry, C. H., van der Veen, D. R., Labeed, F. H., & Hughes, M. P. (2019). Ten-second electrophysiology: Evaluation of the 3DEP platform for high-speed, high-accuracy cell analysis. *Scientific Reports*, 9(1), 19153. <https://doi.org/10.1038/s41598-019-55579-9>
- Hoettges, K. F., Hubner, Y., Broche, L. M., Ogin, S. L., Kass, G. E., & Hughes, M. P. (2008). Dielectrophoresis-activated multiwell plate for label-free high-throughput drug assessment. *Analytical Chemistry*, 80(6), 2063–2068. <https://doi.org/10.1021/ac702083g>
- Hunter, D. J., & Bierma-Zeinstra, S. (2019). Osteoarthritis. *Lancet*, 393(10182), 1745–1759. [https://doi.org/10.1016/S0140-6736\(19\)30417-9](https://doi.org/10.1016/S0140-6736(19)30417-9)
- Inayama, M., Suzuki, Y., Yamada, S., Kurita, T., Yamamura, H., Ohya, S., Giles, W. R., & Imaizumi, Y. (2015). Orai1-Orai2 complex is involved in store-operated calcium entry in chondrocyte cell lines. *Cell Calcium*, 57(5-6), 337–347. <https://doi.org/10.1016/j.ceca.2015.02.005>
- Ismail, A., Hughes, M. P., Mulhall, H. J., Oreffo, R. O., & Labeed, F. H. (2015). Characterization of human skeletal stem and bone cell populations using dielectrophoresis. *Journal of Tissue Engineering and Regenerative Medicine*, 9(2), 162–168. <https://doi.org/10.1002/term.1629>
- Jiang, L. H., Mousawi, F., Yang, X., & Roger, S. (2017). ATP-induced Ca²⁺-signalling mechanisms in the regulation of mesenchymal stem cell migration. *Cellular and Molecular Life Science*, 74(20), 3697–3710. <https://doi.org/10.1007/s00018-017-2545-6>
- Kawano, S., Otsu, K., Shoji, S., Yamagata, K., & Hiraoka, M. (2003). Ca²⁺ oscillations regulated by Na⁺-Ca²⁺ exchanger and plasma membrane Ca²⁺ pump induce fluctuations of membrane currents and potentials

- in human mesenchymal stem cells. *Cell Calcium*, 34(2), 145–156. [https://doi.org/10.1016/s0143-4160\(03\)00069-1](https://doi.org/10.1016/s0143-4160(03)00069-1)
- Koelling, S., Kruegel, J., Irmer, M., Path, J. R., Sadowski, B., Miro, X., & Miosge, N. (2009). Migratory chondrogenic progenitor cells from repair tissue during the later stages of human osteoarthritis. *Cell Stem Cell*, 4(4), 324–335. <https://doi.org/10.1016/j.stem.2009.01.015>
- Kraft, R., Krause, P., Jung, S., Basrai, D., Liebmann, L., Bolz, J., & Patt, S. (2003). BK channel openers inhibit migration of human glioma cells. *Pflugers Archiv: European Journal of Physiology*, 446(2), 248–255. <https://doi.org/10.1007/s00424-003-1012-4>
- Labeed, F. H., Lu, J., Mulhall, H. J., Marchenko, S. A., Hoettges, K. F., Estrada, L. C., Lee, A. P., Hughes, M. P., & Flanagan, L. A. (2011). Biophysical characteristics reveal neural stem cell differentiation potential. *PLoS One*, 6(9), e25458. <https://doi.org/10.1371/journal.pone.0025458>
- Lewis, R., Asplin, K. E., Bruce, G., Dart, C., Mobasher, A., & Barrett-Jolley, R. (2011). The role of the membrane potential in chondrocyte volume regulation. *Journal of Cellular Physiology*, 226(11), 2979–2986. <https://doi.org/10.1002/jcp.22646>
- Lewis, R., & Barrett-Jolley, R. (2015). Changes in membrane receptors and ion channels as potential biomarkers for osteoarthritis. *Frontiers in Physiology*, 6, 357. <https://doi.org/10.3389/fphys.2015.00357>
- Lewis, R., Feetham, C. H., Gentles, L., Penny, J., Tregilgas, L., Tohami, W., Mobasher, A., & Barrett-Jolley, R. (2013). Benzamil sensitive ion channels contribute to volume regulation in canine chondrocytes. *British Journal of Pharmacology*, 168(7), 1584–1596. <https://doi.org/10.1111/j.1476-5381.2012.02185.x>
- Li, W., Wei, S., Liu, C., Song, M., Wu, H., & Yang, Y. (2016). Regulation of the osteogenic and adipogenic differentiation of bone marrow-derived stromal cells by extracellular uridine triphosphate: The role of P2Y2 receptor and ERK1/2 signaling. *International Journal of Molecular Medicine*, 37(1), 63–73. <https://doi.org/10.3892/ijmm.2015.2400>
- Loeser, R. F., Goldring, S. R., Scanzello, C. R., & Goldring, M. B. (2012). Osteoarthritis: A disease of the joint as an organ. *Arthritis and Rheumatism*, 64(6), 1697–1707. <https://doi.org/10.1002/art.34453>
- Mahabadi, S., Labeed, F. H., & Hughes, M. P. (2018). Dielectrophoretic analysis of treated cancer cells for rapid assessment of treatment efficacy. *Electrophoresis*, 39(8), 1104–1110. <https://doi.org/10.1002/elps.201700488>
- Maleckar, M. M., Clark, R. B., Votta, B., & Giles, W. R. (2018). The resting potential and K⁺ currents in primary human articular chondrocytes. *Frontiers in Physiology*, 9, 974. <https://doi.org/10.3389/fphys.2018.00974>
- Maleckar, M. M., Martin-Vasallo, P., Giles, W. R., & Mobasher, A. (2020). Physiological effects of the electrogenic current generated by the Na⁺/K⁺ pump in mammalian articular chondrocytes. *Bioelectricity*, 2, 258–268. <https://doi.org/10.1089/bioe.2020.0036>
- Mankin, H. J., & Lippiello, L. (1971). Biochemical and metabolic abnormalities in articular cartilage from osteo-arthritic human hips. *The Journal of Bone and Joint Surgery American Volume*, 52(3), 424–434.
- Mattà, C., Boockook, D. J., Fellows, C. R., Miosge, N., Dixon, J. E., Liddell, S., Smith, J., & Mobasher, A. (2019). Molecular phenotyping of the surfaceome of migratory chondroprogenitors and mesenchymal stem cells using biotinylation, glyco-capture and quantitative LC-MS/MS proteomic analysis. *Scientific Reports*, 9(1), 9018. <https://doi.org/10.1038/s41598-019-44957-y>
- Mattà, C., Fodor, J., Miosge, N., Takacs, R., Juhasz, T., Rybaltovszki, H., Toth, A., Csernoch, L., & Zakany, R. (2015). Purinergic signalling is required for calcium oscillations in migratory chondrogenic progenitor cells. *Pflugers Archiv: European Journal of Physiology*, 467(2), 429–442. <https://doi.org/10.1007/s00424-014-1529-8>
- Mattà, C., & Zakany, R. (2013). Calcium signalling in chondrogenesis: Implications for cartilage repair. *Frontiers Bioscience*, 5, 305–324. <https://www.ncbi.nlm.nih.gov/pubmed/23277053>
- Mizutani, H., Yamamura, H., Muramatsu, M., Hagihara, Y., Suzuki, Y., & Imaizumi, Y. (2016). Modulation of Ca²⁺ oscillation and melatonin secretion by BKCa channel activity in rat pinealocytes. *American Journal of Physiology: Cell Physiology*, 310(9), C740–C747. <https://doi.org/10.1152/ajpcell.00342.2015>
- Mobasher, A., Lewis, R., Ferreira-Mendes, A., Rufino, A., Dart, C., & Barrett-Jolley, R. (2012). Potassium channels in articular chondrocytes. *Channels*, 6(6), 416–425. <https://doi.org/10.4161/chan.22340>
- Mobasher, A., Lewis, R., Maxwell, J. E., Hill, C., Womack, M., & Barrett-Jolley, R. (2010). Characterization of a stretch-activated potassium channel in chondrocytes. *Journal of Cellular Physiology*, 223(2), 511–518. <https://doi.org/10.1002/jcp.22075>
- Mobasher, A., Mattà, C., Uzielienė, I., Budd, E., Martin-Vasallo, P., & Bernotienė, E. (2019). The chondrocyte channelome: A narrative review. *Joint, Bone, Spine*, 86(1), 29–35. <https://doi.org/10.1016/j.jbspin.2018.01.012>
- Mobasher, A., Mobasher, R., Francis, M. J., Trujillo, E., Alvarez de la Rosa, D., & Martin-Vasallo, P. (1998). Ion transport in chondrocytes: membrane transporters involved in intracellular ion homeostasis and the regulation of cell volume, free [Ca²⁺] and pH. *Histology and Histopathology*, 13(3), 893–910. <https://doi.org/10.14670/HH-13.893>
- Morey, J. S., Ryan, J. C., & Van Dolah, F. M. (2006). Microarray validation: Factors influencing correlation between oligonucleotide microarrays and real-time PCR. *Biological Procedures Online*, 8, 175–193. <https://doi.org/10.1251/bpo126>
- Mow, V. C., Wang, C. C., & Hung, C. T. (1999). The extracellular matrix, interstitial fluid and ions as a mechanical signal transducer in articular cartilage. *Osteoarthritis and Cartilage*, 7(1), 41–58. <https://doi.org/10.1053/joca.1998.0161>
- Nakayama, N., Pothiwala, A., Lee, J. Y., Matthias, N., Umeda, K., Ang, B. K., Huard, J., Huang, Y., & Sun, D. (2020). Human pluripotent stem cell-derived chondroprogenitors for cartilage tissue engineering. *Cellular and Molecular Life Science*, 77(13), 2543–2563. <https://doi.org/10.1007/s00018-019-03445-2>
- Okamoto, T., Aoyama, T., Nakayama, T., Nakamata, T., Hosaka, T., Nishijo, K., Nakamura, T., Kiyono, T., & Toguchida, J. (2002). Clonal heterogeneity in differentiation potential of immortalized human mesenchymal stem cells. *Biochemical and Biophysical Research Communications*, 295(2), 354–361. <https://www.ncbi.nlm.nih.gov/pubmed/12150956>
- Pchelintseva, E., & Djamgoz, M. B. A. (2018). Mesenchymal stem cell differentiation: Control by calcium-activated potassium channels. *Journal of Cellular Physiology*, 233(5), 3755–3768. <https://doi.org/10.1002/jcp.26120>
- Saeed, A., Francini, N., White, L., Dixon, J., Gould, T., Rashidi, H., Al Ghanami, R. C., Hruschka, V., Redl, H., Saunders, B. R., Alexander, C., & Shakesheff, K. M. (2015). A thermoresponsive and magnetic colloid for 3D cell expansion and reconfiguration. *Advanced Materials*, 27(4), 662–668. <https://doi.org/10.1002/adma.201403626>
- Suzuki, Y., Yamamura, H., Imaizumi, Y., Clark, R. B., & Giles, W. R. (2020). K⁺ and Ca²⁺ channels regulate Ca²⁺ signaling in chondrocytes: An illustrated review. *Cells*, 9(7), 1577. <https://doi.org/10.3390/cells9071577>
- Urban, J. P., Hall, A. C., & Gehl, K. A. (1993). Regulation of matrix synthesis rates by the ionic and osmotic environment of articular chondrocytes. *Journal of Cellular Physiology*, 154(2), 262–270. <https://doi.org/10.1002/jcp.1041540208>
- Vaeth, M., Yang, J., Yamashita, M., Zee, I., Eckstein, M., Knosp, C., Kaufmann, U., Karoly Jani, P., Lacruz, R. S., Flockerzi, V., Kacs Kovics, I., Prakriya, M., & Feske, S. (2017). ORAI2 modulates

- store-operated calcium entry and T cell-mediated immunity. *Nature Communications*, 8, 14714. <https://doi.org/10.1038/ncomms14714>
- Wakle-Prabakaran, M., Lorca, R. A., Ma, X., Stamnes, S. J., Amazu, C., Hsiao, J. J., Karch, C. M., Hyrc, K. L., Wright, M. E., & England, S. K. (2016). BKCa channel regulates calcium oscillations induced by alpha-2-macroglobulin in human myometrial smooth muscle cells. *Proceedings of the National Academy of Sciences of the United States of America*, 113(16), E2335–E2344. <https://doi.org/10.1073/pnas.1516863113>
- Wilson, J. R., Duncan, N. A., Giles, W. R., & Clark, R. B. (2004). A voltage-dependent K⁺ current contributes to membrane potential of acutely isolated canine articular chondrocytes. *Journal of Physiology*, 557(Pt 1), 93–104. <https://doi.org/10.1113/jphysiol.2003.058883>
- Zhang, Y. Y., Yue, J., Che, H., Sun, H. Y., Tse, H. F., & Li, G. R. (2014). BKCa and hEag1 channels regulate cell proliferation and differentiation in human bone marrow-derived mesenchymal stem cells. *Journal of Cellular Physiology*, 229(2), 202–212. <https://doi.org/10.1002/jcp.24435>
- Zhao, Y., Wei, H., Kong, G., Shim, W., & Zhang, G. (2013). Hydrogen sulfide augments the proliferation and survival of human induced pluripotent stem cell-derived mesenchymal stromal cells through

inhibition of BKCa. *Cytotherapy*, 15(11), 1395–1405. <https://doi.org/10.1016/j.jcyt.2013.06.004>

SUPPORTING INFORMATION

Additional Supporting Information may be found online in the supporting information tab for this article.

How to cite this article: Matta, C., Lewis, R., Fellows, C., Diszhazi, G., Almassy, J., Miosge, N., Dixon, J., Uribe, M. C., May, S., Poliska, S., Barrett-Jolley, R., Fodor, J., Szentesi, P., Hajdú, T., Keller-Pinter, A., Henslee, E., Labeed, F. H., Hughes, M. P., & Mobasher, A. (2021). Transcriptome-based screening of ion channels and transporters in a migratory chondroprogenitor cell line isolated from late-stage osteoarthritic cartilage. *J Cell Physiol*, 236, 7421–7439. <https://doi.org/10.1002/jcp.30413>